Research Square

Preprints are preliminary reports that have not undergone peer review.
They should not be considered conclusive, used to inform clinical practice,
or referenced by the media as validated information.

Volcano-like b-value rise without volcanic heat beneath the 2020–2024 Noto Peninsula swarm, Japan

RamaKrishna Pasupuleti

workisfun415@gmail.com

Kakatiya University https://orcid.org/0009-0008-8418-1430

Rithwik Mittal

Mahindra École Centrale https://orcid.org/0009-0004-6259-2416

P.J.V.Ram

Independent Researcher https://orcid.org/0009-0006-5899-5284

Research Article

Keywords: Noto Peninsula, earthquake swarm, b-value, magnitude–frequency distribution, brittle–ductile transition, catalogue processing, b-value precursor, reproducibility

Posted Date: November 13th, 2026

DOI: https://doi.org/10.21203/rs.3.rs-11709341/v1

License: This work is licensed under a Creative Commons Attribution 4.0 International License.
Read Full License

Additional Declarations: The authors declare no competing interests.

Volcano-like b-value rise without volcanic heat beneath the 2020–2024 Noto Peninsula swarm, Japan

Ramakrishna Pasupuleti[1]*, Ritvik Mittal[2], P.J.V.Ram[3]

[1] Independent Researcher, Suryapet, Telangana, India

[2] Mahindra University, Hyderabad, Telangana, India

[3] Independent Researcher, Hyderabad, Telangana, India

* Corresponding author: workisfun415@gmail.com

ORCID: R. Pasupuleti 0009-0008-8418-1430; R. Mittal 0009-0004-6259-2416; P.J.V.Ram 0009-0006-5899-5284

Abstract

Departures of earthquake magnitude–frequency distributions (FMDs) from the Gutenberg–Richter law may reflect source physics or catalogue processing. In the relocated catalogue of the 2020–2024 Noto Peninsula swarm, events deeper than 13 km follow a two-slope law (b_1 = 1.57, b_2 = 0.75; ΔBIC = −107). After correcting the Japan Meteorological Agency (JMA) M 1.7 processing step, the break vanishes at 10–13 km but survives below 13 km, where a steep population (b ≈ 1.7) rises from ≤ 2% to 33–60% of events within 1 km and persists from 2021 to late 2023. An event-level mixture model maps the depth z50 at which this population takes over, a proxy of the brittle–ductile transition, at 12.45–13.5 km; it varies laterally, deepens 4.3° to the SE and is reproduced by the JMA catalogue. The steep population lies 3–5 km into the footwall of the Suzu blind fault rather than on it, and it is no less clustered in time than the layer above. With one pre-registered rule applied to JMA data across Japan, b falls below the local base of seismicity in all seven testable non-volcanic units before 2016; after 2016 similar signals elsewhere arise from automatic hypocentres, whereas at Noto the signal is strongest in reviewed events (Δb = +1.6). Near the active volcanoes of NE Japan b rises below the base (Δb = +0.73; +0.84 without low-frequency earthquakes), but not in non-volcanic crust; in Kyushu and Hokkaido the rise is weaker (+0.42) and inconclusive once low-frequency earthquakes are removed. Noto, which has no active volcano and no low-frequency earthquakes, shows a stronger rise at a base of seismicity about 5 km deeper than near the volcanoes: a volcanic-type signature that we tentatively attribute to high fluid pressure from a deep source rather than to high temperature; surface heat flow at Noto is lower than near the volcanoes. A reported b-value precursor of the 2024 Mw 7.5 fails a false-alarm test. All tests were pre-specified or are labelled post hoc.

Keywords: Noto Peninsula; earthquake swarm; b-value; magnitude–frequency distribution; brittle–ductile transition; catalogue processing; b-value precursor; reproducibility

Key points

- After correcting a JMA processing step, the deep FMD kink of the Noto swarm survives and is produced by a steep small-event population ($b \approx 1.7$) below a laterally varying brittle–ductile transition proxy ($z50 \approx 12.5$–13.5 km).
- Across Japan the same rule finds b falling below the base of seismicity in non-volcanic crust but rising near the active volcanoes of NE Japan (also without low-frequency earthquakes; weaker and inconclusive in Kyushu and Hokkaido); Noto shows the strongest rise of all, a volcanic-type signature in a non-volcanic swarm.
- The steep population lies below, not on, the Suzu blind fault; its relation to the 2024 Mw 7.5 is not established, and the reported b-value precursor fails a false-alarm test.

1. Introduction

The slope b of the Gutenberg–Richter (GR) law, $\log_{10} N(M \geq m) = a - b\,m$ (Gutenberg and Richter 1944), is used as a proxy for differential stress (Scholz 1968; Schorlemmer et al. 2005) and to discriminate foreshocks from aftershocks (Gulia and Wiemer 2019). These uses assume that one straight line describes the magnitude–frequency distribution (FMD) above completeness. Curved or broken FMDs can arise from incompleteness, magnitude scaling of small events (Deichmann 2006; Uchide and Imanishi 2018), heterogeneous catalogue processing (Tamaribuchi 2018) or physical changes with depth (Spada et al. 2013).

Changes of b with depth are not new. b decreases with depth in California (Mori and Abercrombie 1997), rises towards the base of the seismogenic layer in some regions (Spada et al. 2013) and is high beneath volcanoes (Wiemer and McNutt 1997), and the brittle–ductile transition is commonly placed at the base of seismicity. What is less established is how to separate such physical changes from the effects of catalogue processing in a modern catalogue that mixes reviewed and automatic hypocentres, how to map them in three dimensions from magnitudes alone, and whether one rule applied to many areas finds them only in particular settings. These are the aims of this study.

The 2020–2024 swarm beneath the northeastern Noto Peninsula preceded the 1 January 2024 Mw 7.5 earthquake and is one of the best-documented fluid-driven swarms. A low-velocity lower crust suggests fluid supply from depth (Nakajima 2022); hypocentres migrated diffusively and upward from a deep ring-shaped cluster (Amezawa et al. 2023; Yoshida, Uno et al. 2023); geodesy shows tensile opening at about 16 km followed by aseismic slip (Nishimura et al. 2023), in an aseismic zone at 14–16 km (Takano et al. 2024); the 2023 Mj 6.5 ruptured a ~45° SE-dipping fault (Kato 2024); and the Mw 7.5 started on the SE-dipping Suzu blind fault at the front of the migration (Yoshida et al. 2024) and broke a strong asperity at the edge of the swarm (Xu et al. 2024). Hirose et al. (2024) found a high b-value (1.85) in the deepest cluster, and Li et al. (2024) reported a b-value rise before the Mw 7.5. Mantle helium near the source region indicates fluids of deep origin (Umeda et al. 2024; Kagoshima et al. 2025).

We show that the FMD of this swarm breaks below 13 km, separate a catalogue-processing effect from a physical one, and use the physical part to map a brittle–ductile transition proxy in three dimensions. We ask: (1) Is the break real, and which part survives correction of the JMA processing step? (2) Can the depth at which the steep population takes over be mapped laterally, and does an independent catalogue reproduce it? (3) How does this transition relate to the seismicity-poor zone, the faults and the large earthquakes? (4) Does the reported b-value precursor

survive a false-alarm test? (5) Is the steep population unique to Noto, and in which settings does it occur elsewhere in Japan? Every analysis was specified in a protocol fingerprinted with SHA-256 before it was run; analyses added after seeing results are labelled post hoc.

2. Data

We use the double-difference relocated catalogue of Yoshida et al. (2024; doi 10.5281/zenodo.12799165; CC BY 4.0), which contains 31,158 events of M_JMA ≥ 1 from 2003 to March 2024 with a mean 95% relative depth uncertainty of about 0.13 km. The main set contains 14,810 events of M ≥ 1.2 in 2021–2023 (1,787 shallower than 10 km, 9,993 at 10–13 km, 3,030 at ≥ 13 km); the transition map uses the 9,576 events from 1 January 2021 to the 2023 Mj 6.5. The Mw 7.5 is not in the catalogue; the M 5.9 at 16:10:09 is its pre-event (Aochi 2024). Since April 2016 the JMA unified catalogue flags each hypocentre as fully checked, simply checked or automatic; on land the threshold between these classes is M_th = 1.7 (Tamaribuchi 2018). We matched 6,437 relocated events of M ≥ 1.5 one-to-one to the JMA catalogue. For replication and comparison we use the JMA catalogue of the swarm (M ≥ 1.5), of the Ibaraki and Nankai regions, four other pre-mainshock sequences (Karimpouli et al. 2026; GFZ Data Services), the Vs model of Takagi, Yoshida and Okada (2025), the Vp and Vs model of Nakajima (2022) and helium data of Kagoshima et al. (2025). For comparisons across Japan we use JMA unified-catalogue extracts (2000–2024) of the Wakayama swarm, northern Yamaguchi, the Yamagata–Miyagi region, the Tohoku box 35–41°N, 140–146°E, and boxes around 13 active volcanoes in Kyushu and Hokkaido.

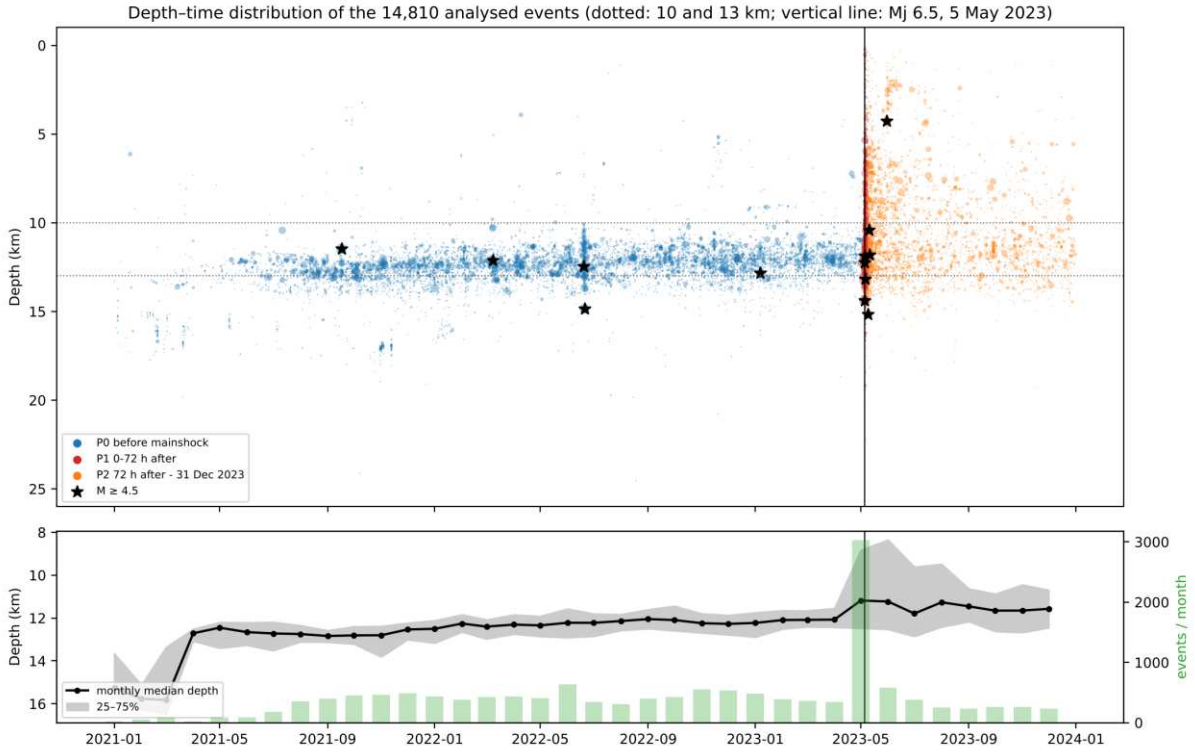


Figure 1. Depth–time distribution of the 14,810 analysed events (blue before, red 0–72 h after and orange later than the 2023 Mj 6.5; stars M ≥ 4.5) and monthly median depth and event count. Dotted lines: 10 and 13 km.

3. Methods

3.1 FMD models

Completeness by maximum curvature + 0.2 and goodness of fit (Wiemer and Wyss 2000) is ≤ 1.2 in all depth bands, and M_c = 1.2 is used unless stated. b is the maximum-likelihood estimate (Aki 1965; Utsu 1965) with the uncertainty of Shi and Bolt (1982). With $m_0 = M_c - 0.05$ we compare a single law, a broken law and a two-population mixture:

$$S_1(m) = 10^{-b(m - m_0)} \quad \text{(single law)}$$

$$S_2(m) = 10^{-b_1(m - m_0)} \text{ for } m < M_k; \quad 10^{-b_1(M_k - m_0) - b_2(m - M_k)} \text{ for } m \geq M_k \quad \text{(broken law)}$$

$$S_3(m) = w \cdot 10^{-b_a(m - m_0)} + (1 - w) \cdot 10^{-b_b(m - m_0)} \quad \text{(mixture)}$$

using the binned likelihood $\ln L = \Sigma\, n_v \ln[S(v - 0.05) - S(v + 0.05)]$ and $BIC = k \ln N - 2 \ln L$. A break is called present if $\Delta BIC < -10$ and a parametric bootstrap that repeats the full search for M_k gives $p < 0.05$; in 4,000 simulated single-law catalogues no case reached $\Delta BIC < -10$.

3.2 The processing step and its correction

The step was measured outside Noto. In the JMA catalogue of the Ibaraki and Nankai regions the share of M 1.5 and 1.6 events relative to M ≥ 1.7 increased after April 2016 by the factors f(1.5) = 1.89 (95% CI 1.77–2.01) and f(1.6) = 1.86 (1.74–1.99). Noto counts at M ≤ 1.6 were weighted

by 1/f. The pre-registered prediction was that the break at 10–13 km disappears while the steep component at 13–14 km survives.

Robustness was tested by perturbing all depths (Gaussian noise of 0.13–1.0 km; shifts of ±0.5 and ±1 km), by five pairs of depth boundaries, by nearest-neighbour declustering (Zaliapin and Ben-Zion 2013), with a single magnitude type and by year. The same model comparison was applied to four other pre-mainshock sequences at the completeness given by the data authors and at a conservative value. In depth slices of 0.5–1 km of the northern cluster, an end-member mixture with both slopes fixed from pure groups and only the weight w free (k = 1) measured the share of the steep population. Depth–b profiles were computed for the same events with JMA and relocated depths, and the JMA–relocated depth difference was compared between processing classes. Tidal sensitivity was tested with TidalStrain.2 (Hirose et al. 2019) and the Schuster (1897) statistic, with a clustering-preserving time-shift null added after the first results.

3.3 Event-level mixture and three-dimensional map

Each event i of magnitude $m_i \geq M_c$ and depth z_i belongs to a steep population with probability $w(z_i)$ and to a brittle population otherwise, with w changing with depth as a logistic function centred on z50:

$$w(z) = 1 / (1 + \exp(-(z - z50)/s))$$

$$P_i = w(z_i)\, p_{high}(m_i) + (1 - w(z_i))\, p_{low}(m_i), \quad p(m) = \beta\, e^{-\beta(m - M_c)}\, \Delta m, \quad \beta = b \ln 10$$

$$\ell(z50) = \Sigma_i\, c_i \ln P_i, \quad c_i = 1/f \text{ for } m_i < 1.7, \text{ otherwise } 1$$

$b_{low} = 0.88$, $b_{high} = 1.72$ and $s = 0.25$ km were estimated once from all 9,576 events (global z50 = 13.35 km) and held fixed. At each node of a 1-km grid in coordinates rotated to the strike of the Suzu fault (53°; origin 37.5°N, 137.25°E) we used the events within a radius growing from 2.5 to 4 km until $N \geq 300$ and maximised ℓ on a 0.05-km grid; 90% intervals come from 200 bootstrap resamples. A node is well constrained (post hoc rule) if its profile interval is ≤ 1.5 km and ≥ 20 events lie within ±0.5 km of z50. Lateral variation was tested with the gain $G = 2\, \Sigma_{tiles} [\ell_{tile}(\hat{z}50,tile) - \ell_{tile}(\hat{z}50,global)]$ over 5-km tiles against 200 permutations of magnitudes within 0.5-km depth bins. Synthetic catalogues with the real hypocentres and a flat (13.2 km) or dipping (12.7–13.7 km) surface tested the method. The same code was applied unchanged to the JMA catalogue ($M \geq 1.5$, N = 4,084) with four pre-specified tests: J1 lateral variation, J2 the same pattern at common nodes, J3 a deeper transition beneath the eastern cluster, J4 the SE deepening. Maps are drawn with NW up and sections as seen from the SW.

3.4 Test of a b-value precursor

Consecutive 90-day blocks ending at each mainshock were compared with the preceding block by the Utsu (1992) test,

$$\Delta AIC = -2(N_1 + N_2) \ln(N_1 + N_2) + 2N_1 \ln(N_1 + N_2\, b_1/b_2) + 2N_2 \ln(N_2 + N_1\, b_2/b_1) - 2,$$

with $\Delta AIC > 2$ regarded as significant, in four pre-specified settings: S1, M_c = 1.4 (maximum curvature + 0.2) at all depths, as in the published approach; S2, M_c = 1.8; S3, M_c = 1.2 with step-corrected counts; S4, M_c = 1.8 within 10–13 km only. The false-alarm rate is the share of ordinary blocks passing the same threshold. A precursor is supported only if S2–S4 are significant and the false-alarm rate is low.

3.5 Comparison across Japan and with volcanic areas

To compare areas with one rule (R2, pre-registered), we computed the local base D90 (the 90% depth of seismicity on a 1-km grid, radius 2–4 km until $N \geq 300$, all magnitudes) and the relative depth h = depth − D90 of each event shallower than 30 km, and compared b below the base with b just above it:

$$\Delta b = b(h \geq +1 \text{ km}) - b(-3 \leq h < -1 \text{ km})$$

with Aki–Utsu b at $M \geq M_c$ (maximum curvature + 0.2) and 2,000 bootstrap resamples. A unit is Noto-type if $\Delta b \geq 0.4$, the 95% interval excludes zero and $b(h \geq +1) \geq 1.3$, and insufficient if either band has fewer than 150 events. Noto (2021 to the Mj 6.5) served as positive control; units were whole areas and every JMA region name with ≥ 1,000 events. Three pre-registered follow-ups tested (T1) the same rule in the same era as Noto (2016–2024), (T2) its power, by thinning Noto at random to the size of each comparison unit (100 thinnings), and (H-V) whether the signal is stronger near volcanoes. For H-V, volcanic events lie within 15 km of an active volcano and non-volcanic events are onshore crustal events more than 30 km from all of them; the statistic uses reviewed events only (JMA flags k, s, K, S) after 2016 (primary) and all events before 2016, when every hypocentre was reviewed. The decision required $\Delta b_volc \geq 0.4$ and $\Delta b_volc - \Delta b_non \geq 0.3$, both with intervals excluding zero, and each depth band needed at least 40 reviewed events. Moriyoshi-zan, where the idea arose, was excluded; the test was then repeated unchanged in Kyushu and Hokkaido, removing the 2016–2017 Kumamoto sequence as declared in advance. Two further pre-registered tests asked whether the steep population lies on the Suzu blind fault (SBF; strike 53°, dip 43° SE; Yoshida et al. 2024) and whether it is less clustered in time than the busy layer, using nearest-neighbour distances (Zaliapin and Ben-Zion 2013) against a time-shuffled null and the local variation of inter-event times (Shinomoto et al. 2003). JMA marks low-frequency earthquakes (LFEs) in the subsidiary information of each hypocentre; because LFEs

near volcanoes may follow a different magnitude–frequency law, the volcanic tests were repeated without them, and the median local base D90 of each group was compared (both post hoc).

To check whether D90 tracks crustal temperature, we compared it with surface heat flow from the Global Heat Flow Database (Global Heat Flow Data Assessment Group et al. 2024; onshore sites, one value per site). The pre-registered test compared median heat flow within 50 km of the swarm with that within 15 km of the NE Japan volcanoes and in non-volcanic NE Japan, and correlated heat flow with the D90 of the nearest node within 5 km (Spearman); each group needed at least five sites.

4. Results

4.1 A robust break below 13 km

Table 1. FMD model comparison (M_c = 1.2, 2021–2023) before and after weighting the counts at M ≤ 1.6 by 1/f. Negative ΔBIC favours the broken or mixture model.

Depth band	N	b (Aki)	b_1 / b_2	M_k	ΔBIC broken / mixture	Bootstrap p	ΔBIC after step correction
Shallow < 10 km	1,787	0.92 ± 0.02	—	—	+12.5 / +15.0	0.47	−4.5
Middle 10–13 km	9,993	1.05 ± 0.01	1.11 / 0.84	1.8	−96.8 / −67.1	< 0.005	+14.5
Deep ≥ 13 km	3,030	1.45 ± 0.03	1.57 / 0.75	1.9	−107.3 / −111.8	< 0.005	−42.0
All depths	14,810	1.09	1.17 / 0.84	1.8	−202.7 / −162.3	< 0.005	—

Shallow events follow a single GR law; middle and deep events strongly prefer a broken or mixture model (Table 1, Fig. 2). A single law fitted to the deep band predicts 7.6 events of M ≥ 3 against 37 observed. The deep break is insensitive to depth errors (Gaussian noise up to 1 km and shifts of ±1 km: bend in all runs), to the depth boundaries, to nearest-neighbour declustering (Zaliapin and Ben-Zion 2013), to a single magnitude type, and to the year (2021, 2022 and 2023 separately); it existed before the 2023 Mj 6.5 (Table 2; Fig. 1). The deep southern cluster, where Hirose et al. (2024) found b = 1.85, follows a single steep law (b ≈ 1.7, M_max 2.6), and removing it leaves the deep break unchanged; the break lies mainly in the northern cluster at 12–14 km. Four other pre-mainshock sequences (L'Aquila, Amatrice, Kahramanmaraş, Iquique) show no break of this shape (Table 3).

A plane fitted to the first 72 h of aftershocks of the 2023 Mj 6.5 dips 37° towards 151°; it is shallower than the ~45° of Kato (2024) because one plane is fitted to two parallel faults and to poorly located offshore events (39° before the Mj 5.9 aftershock), and it is used only to classify events. Before the mainshock 64% of events lie within 1.5 km of this plane, against 19% for randomly oriented planes through the same centroid, so the swarm was preferentially organised

along the future rupture. Below 13 km the two sides differ: events on the plane bend, whereas events off it lie deeper (median 15.1 km) and below 14 km follow a single steep law (b = 1.91) with no event of M ≥ 3; events of M ≥ 4 deeper than 12 km are about three times more frequent on the plane (Fisher p = 0.06). The two populations therefore meet where the base of the fault reaches the steep population, at 13–14 km, where Kato (2024) placed the initiation of the 2023 rupture.

Table 2. Robustness of the break (M_c = 1.2 unless stated).

Test	Result for the deep break
Depth noise 0.13, 0.5, 1.0 km (50 runs each)	Bend in 100% of runs (median ΔBIC −114 to −118); shallow never
Depth shift ±0.5, ±1 km	Bend in all (ΔBIC −35 to −197)
Five boundary pairs 8/11 … 12/15 km	Deepest group bends in all; groups entirely above 11 km never
Declustering (nearest neighbour), catalogue B / C	ΔBIC −102.9 (mixture) / −34.2 (broken)
Single magnitude type (V only, M ≥ 1.5)	Mixture ΔBIC −35.5; M ≥ 3: 26 observed / 8 expected
Each year 2021, 2022, 2023 (deep)	ΔBIC −14.6, −24.6, −46.6
Before the 2023 Mj 6.5: middle / deep	ΔBIC −83.7 / −57.2 (2021 and 2022 separately also bend)
0–72 h after the Mj 6.5	no bend (short-term incompleteness)
Southern cluster ≥ 14 km (Sd) / N cluster ≥ 14 km	single steep laws, b 1.69 / 2.80
N + E + W clusters, deep (S removed)	ΔBIC −107.2
Above M_th (M_c = 1.7), shallow / middle / deep	ΔBIC +9.5 / +4.7 / −18.6 (b ≈ 0.86 shallow and middle)

Table 3. Replication on other pre-mainshock sequences (Karimpouli et al. 2026; GFZ Data Services). Breaks with $b_1 < b_2$ at the lowest allowed value indicate incompleteness.

Sequence	N (pre-mainshock)	Authors' M_c → ΔBIC, shape	Conservative M_c → ΔBIC	Noto-type break?
L'Aquila 2009	4,075	1.5 → −338, $b_1 < b_2$	1.9 → +12.2	No
Amatrice 2016	12,357	1.8 → +2.7	2.1 → +7.1	No
Kahramanmaraş 2023	5,686	1.0 → −87, $b_1 < b_2$	1.3 → +8.0	No
Iquique 2014	5,398	1.5 → −2.1	1.9 → +4.2	No
Noto 2021–23, deep	3,030	1.2 → −107, $b_1 > b_2$	—	Yes

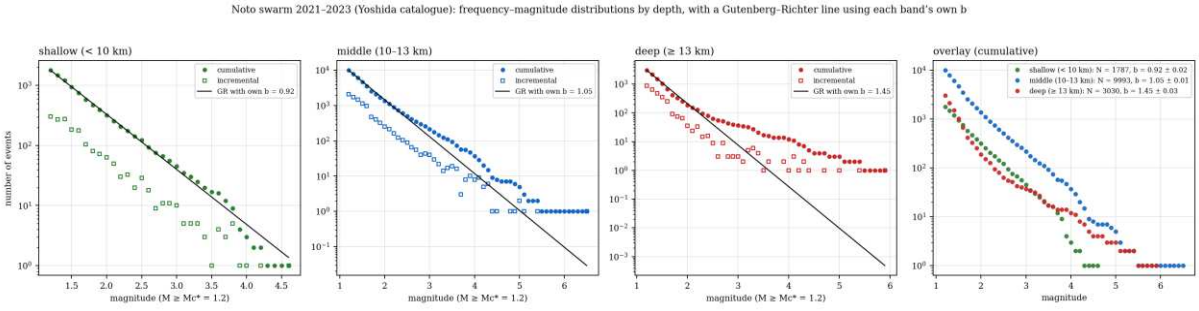


Figure 2. Frequency–magnitude distributions of the relocated catalogue by depth band (M ≥ 1.2, 2021–2023): cumulative (dots) and per-bin (squares) counts with the single GR line of each band. Right: overlay of the three bands.

4.2 The processing step explains the break above 13 km only

Automatic hypocentres make up 65–82% of events at M 1.5–1.6 and none at M ≥ 1.7 in every depth band, year and period. Across M_th the count drops far more than a GR law allows (r = n(1.7)/n(1.6) = 0.36–0.58 against 0.81–0.82 expected), and the same drop appeared in April 2016 in the Ibaraki and Nankai regions, far from Noto (Fig. 3); an unrestricted search places the break

at M 1.7. With the externally measured step removed, the middle band follows a single law (ΔBIC +14.5; +9.2 with the upper-CI factor), whereas the deep band still bends (ΔBIC −42.0; −38.0) (Table 1, Fig. 5). Above M_th the shallow and middle bands follow single laws with b ≈ 0.86.

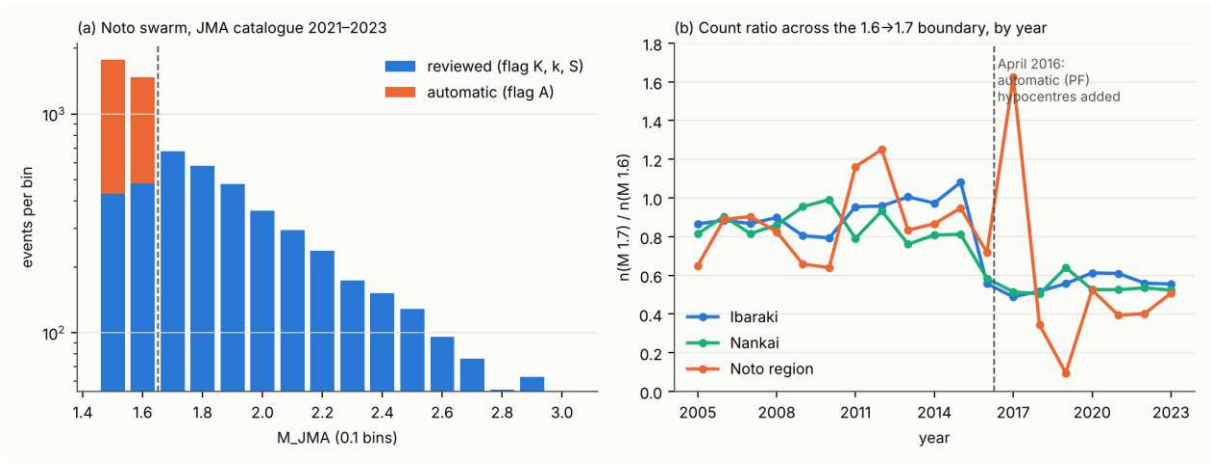


Figure 3. (a) Processing classes of the swarm events in the JMA catalogue; automatic hypocentres occur only below M_th = 1.7. (b) Count ratio n(1.7)/n(1.6) by year in three JMA regions; it fell when automatic hypocentres were introduced in April 2016.

In depth slices of the northern cluster before the 2023 mainshock, the weight w of a steep end member (b fixed to the slope of the pure deep population) is 0.00–0.02 at 10–13 km after the correction, 0.33 (0.22–0.43) at 13–13.5 km and 0.60 (0.47–0.74) at 13.5–14 km, and b_1 increases by 0.44 (0.35–0.56) from 12–13 to 13–14 km (Table 4, Figs. 4–5). The pre-registered survival rule was met for all corrections. The automatic share (0.73–0.86) and the number of stations (19–20) do not change down to 14 km, so a processing effect that changes at 13 km is not supported. Leakage of deeper events cannot supply the 923 excess small events at 13–14 km (157 events lie below 14 km), and smooth b-gradients of 0.23–0.40 per km never produce the observed break in simulations. The remaining explanation is two populations mixing near the brittle–ductile transition, consistent with the regional cutoff depth of about 13 km (Omuralieva et al. 2012) and with the rise of b towards the transition reported by Spada et al. (2013); in Section 4.8 we show, however, that such a rise is not general in the non-volcanic crust of Japan.

Because the steep population was found only in data recorded after automatic hypocentres were introduced, we tested whether automatic locations create it (pre-registered). Among matched events of M 1.5–1.6, automatic events are not placed below the local z50 more often than simply checked (reviewed) events (12.0% against 14.2%; ratio 0.85, 95% CI 0.64–1.16), and the reviewed events alone show the excess of small events below z50: the ratio of M 1.5–1.6 to M ≥ 1.7 events rises by a factor of 4.0 (2.6–6.1) from above to below z50, close to the factor of ≈ 2.4 expected for b ≈ 1.7. Relative to relocated depths, automatic events below z50 are placed 0.16 km

shallower by JMA, not deeper. Automatic hypocentres therefore do not produce the steep population. A caveat from the Japan-wide comparison (Section 4.8): measured with bands of depth relative to the local base ($h \geq +1$ km against $-3 \leq h < -1$ km) rather than relative to z50, automatic events are over-represented below the base at Noto (ratio 1.20) as much as elsewhere; the decisive evidence is therefore that the steep population persists in reviewed events alone ($\Delta b = +1.24$ to $+1.61$).

Table 4. Northern cluster before the 2023 mainshock by depth slice: broken-model fit and weight w of the steep end member before and after the processing-step correction. The ≥ 14 km group is the steep end member itself.

Slice (km)	N	M_max	b_1 / b_2	ΔBIC broken	w uncorrected (95%)	w step-corrected (95%)
10–12	1,501	4.2	1.15 / 0.83	−4.9	0.04 (0.00–0.11)	0.00–0.02
12–12.5	1,728	5.4	1.18 / 0.79	−25.3	0.04 (0.00–0.11)	0.00–0.02
12.5–13	1,281	4.5	1.17 / 0.79	−9.3	0.05 (0.00–0.14)	0.00–0.02
13–13.5	710	4.2	1.54 / 0.75	−15.6	0.40 (0.29–0.50)	0.33 (0.22–0.43)
13.5–14	367	4.3	1.88 / 0.44	−2.8	0.65 (0.52–0.77)	0.60 (0.47–0.74)
≥ 14	157	1.7	2.80 (single)	+10.1	1.00	1.00

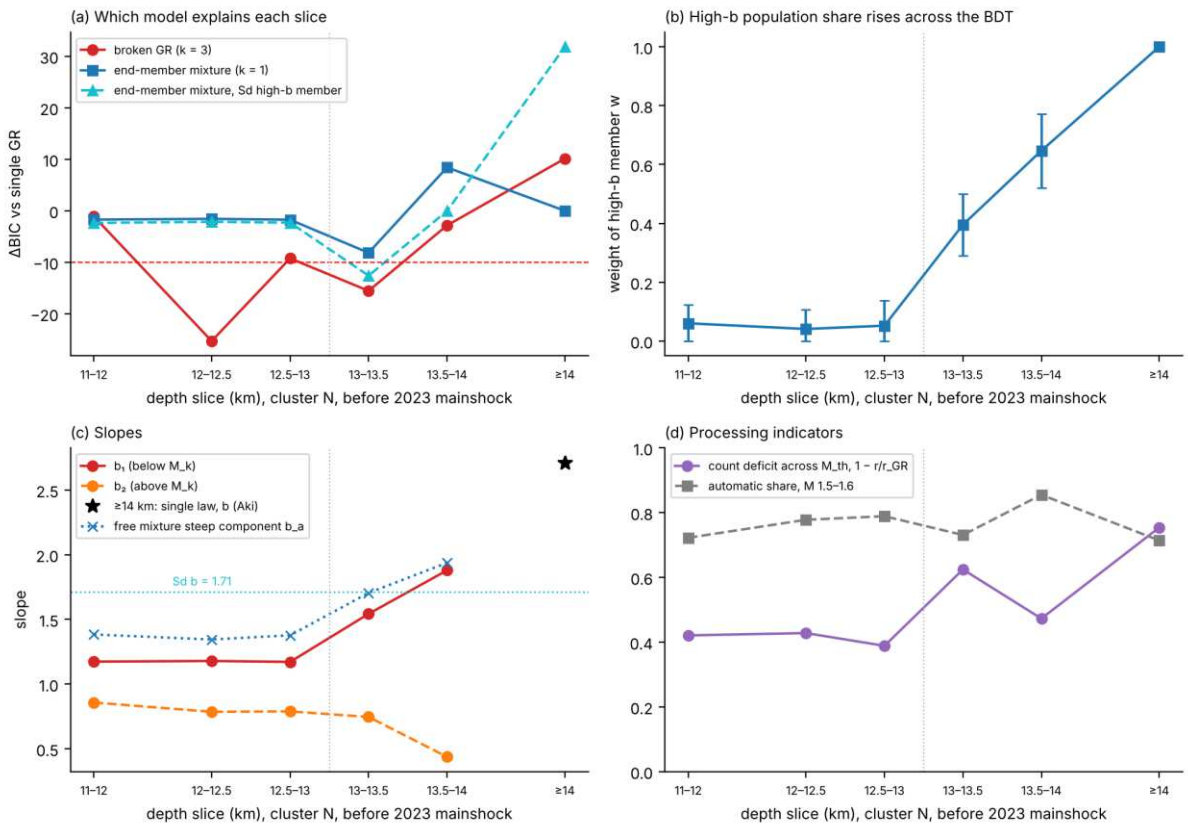


Figure 4. Northern cluster before the 2023 mainshock by depth slice: (a) ΔBIC of the broken (k = 3) and end-member mixture (k = 1) models; (b) weight of the steep end member with 95% bootstrap interval; (c) slopes; (d) count deficit across M_th and automatic share. Dotted line: ≈ 13 km.

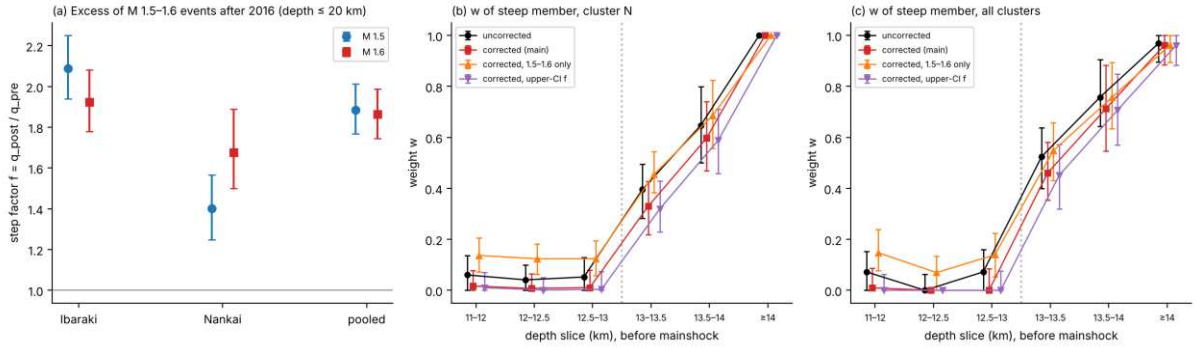


Figure 5. (a) Step factor of M 1.5 and 1.6 events after April 2016 in Ibaraki, Nankai and pooled. (b, c) Weight of the steep end member by depth slice before the 2023 mainshock, uncorrected and with three corrections, for the northern cluster and all clusters. Dotted line: ≈ 13 km.

4.3 Persistence in time

The steep population at 13–14 km was present in every 250-event window from January 2021 to October 2023 (w = 0.22–0.85; Table 5, Fig. 6). It was absent in the first 72 h after the 2023 Mj 6.5 and after the 2024 Mw 7.5 (to March 2024), when small events were missing from the catalogue, so a physical change and incomplete detection cannot be separated after the mainshocks (cf. Mohanna et al. 2026). The last 250 events before each large sequence had w = 0.61–0.91, not different from random times (pre-specified test, p = 0.79), so w is not a precursor.

Table 5. Break by period relative to the two mainshocks (M_c = 1.2). Size control: ΔBIC of 200 random pre-mainshock subsamples of the same size.

Period (all depths)	N	ΔBIC (b_1 / b_2)	Size control: median (% < −10)	Reading
Before 2023 Mj 6.5	9,615	−170.3 (1.26 / 0.85)	—	break
0–72 h after Mj 6.5	1,741	+10.3 (0.80 / 0.64)	−19.0 (81%)	no break; first 6 h incomplete
72 h – 31 Dec 2023	3,455	−18.9 (1.17 / 0.90)	−52.0 (100%)	weaker break; w(13–14 km) 0.68
0–7 d after Mw 7.5	1,807	$b_1 < b_2$	—	incompleteness shape
7 d – 31 Mar 2024	3,683	+3.9 (0.92 / 1.06)	−56.4 (100%)	no break of the Noto shape

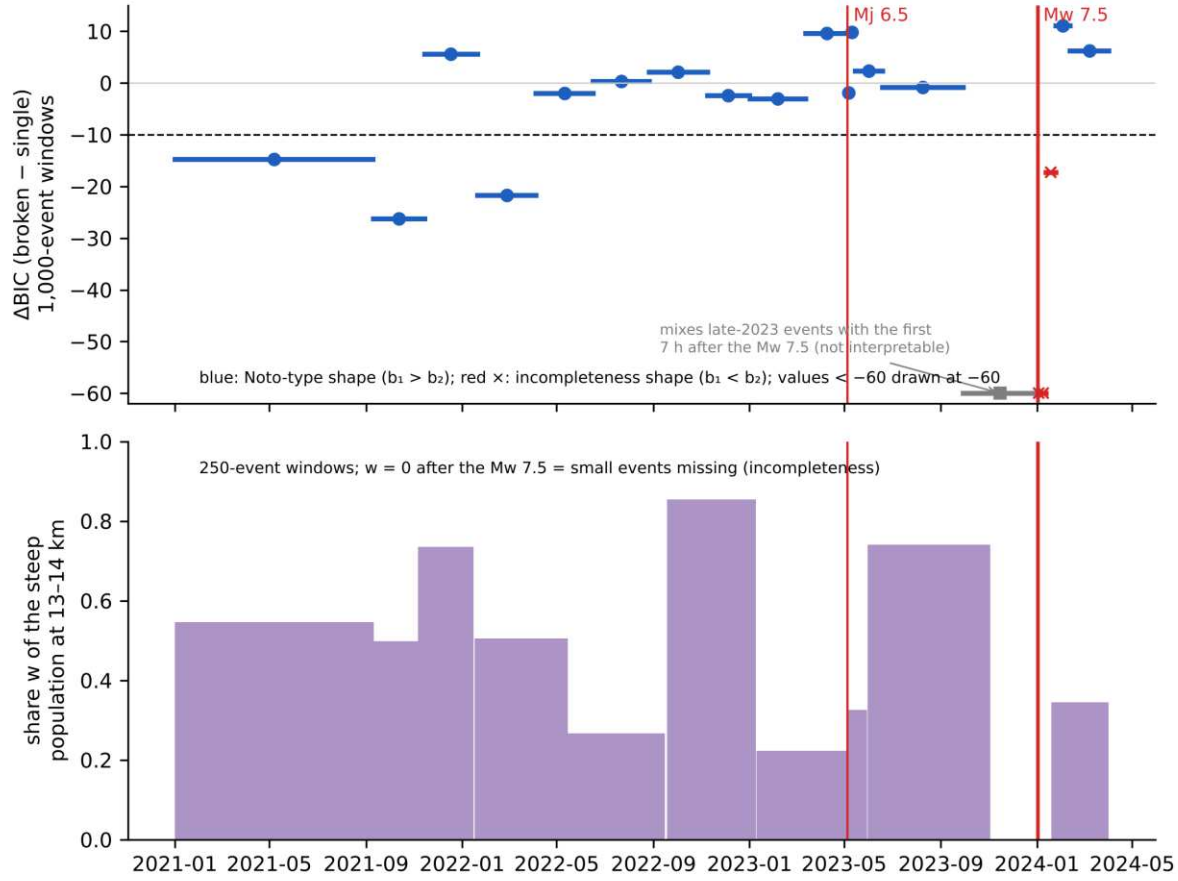


Figure 6. (a) Break strength in consecutive 1,000-event windows (blue: break of the Noto shape; red ×: incompleteness shape). (b) Weight w of the steep population at 13–14 km in consecutive 250-event windows; the window ending on 5 January 2024 (w = 0) consists mainly of events after the Mw 7.5. Vertical lines: 2023 Mj 6.5 and 2024 Mw 7.5.

4.4 A three-dimensional map of the transition

Table 6. The transition proxy z50 in two independently located catalogues. G: likelihood gain of tile-wise z50 against the permutation null (95th percentile).

Quantity	Relocated catalogue	JMA catalogue	Status
Events used; M_c	9,576; 1.2	4,084; 1.5	
b_low / b_high; width s	0.88 / 1.72; 0.25 km	1.06 / 1.81; 0.05 km	
Well-constrained nodes	90 of 236	88 of 170	post hoc rule
z50 median (10–90%)	13.15 km (12.45–13.5)	13.95 km (13.54–14.15)	offset 0.9 km
Lateral variation (tile test)	G 14.55 vs 5.93; p < 0.005	G 2.95 vs 2.39; p = 0.01	replicated (J1)
Same pattern at common nodes	—	ρ = 0.67, n = 63, p = 1×10⁻⁹	replicated (J2)
Eastern cluster deeper than centre	≈ 13.9 vs 13.1 km (tiles)	−0.07 km (90% CI −0.20 … 0.05)	not replicated (J3)
SE deepening of z50	0.075 ± 0.012 km/km (4.3°)	0.058 ± 0.011 km/km	replicated (J4)
Constant-depth control	p = 0.985 (synthetic)	p = 0.985	no false detection

Of 236 nodes, 126 locate z50 and 90 are well constrained. There z50 ranges from 12.1 to 13.85 km (10–90%: 12.45–13.5 km; median 13.15 km) and differs between tiles more than in any permutation (G = 14.55 against a null 95th percentile of 5.93; Table 6, Fig. 7). The method neither creates nor removes lateral variation: a flat synthetic surface is recovered with a median absolute error of 0.15 km and no false detection (p = 0.985), and a dipping one with the same error and

detected ($p < 0.005$). Single nodes scatter by about ±0.5 km, so only patterns spanning several nodes are interpreted (Supplementary Figs. S4, S7).

The most robust feature is a gentle deepening to the SE across strike, 0.075 ± 0.012 km per km (4.3°; $p = 5 \times 10^{-9}$): absent in the SW part of the swarm (−0.047 ± 0.024 km/km), moderate in the centre (+0.063 ± 0.013) and about twice as steep near the 2023 Mj 6.5 (+0.155 ± 0.017 km/km, ≈ 9°). The JMA catalogue reproduces the lateral variation (J1, $p = 0.01$), the pattern (J2, $\rho = 0.67$) and the SE deepening (J4, $p = 5 \times 10^{-7}$), with z50 0.9 km deeper; this offset is larger than the depth offset of the hypocentres (0.17 km for matched events, 0.27 km for D90) and more likely reflects the higher completeness and different mixture parameters of the JMA fit; a deeper transition beneath the eastern cluster is not reproduced (J3) and is not interpreted.

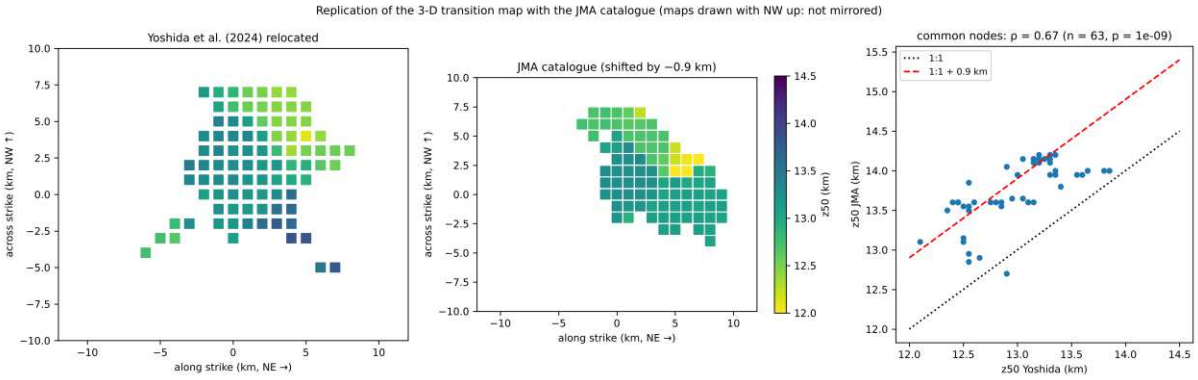


Figure 7. Maps of the transition proxy z50 on a 1-km grid in rotated coordinates (along strike 53°, NE to the right; NW up): (left) relocated catalogue, well-constrained nodes; (centre) JMA catalogue shifted by −0.9 km; (right) z50 at common nodes with the 1:1 line and the 1:1 line plus the median offset.

The transition is sharp. Referred to the local z50, the steep share is 0.02 at 0.5–1 km above, 0.19 at 0–0.5 km above, 0.89 at 0–0.5 km below and 0.96 at 0.5–1 km below, and b changes from 0.88 to 1.67 (Fig. 8). Because z50 is fitted to the same events, we mapped z50 from one random half of the events and measured w with the other half (post hoc); w still rises from 0 to 0.11, 0.40, 0.84 and 1.0 between 1.5 km above and 1 km below the surface.

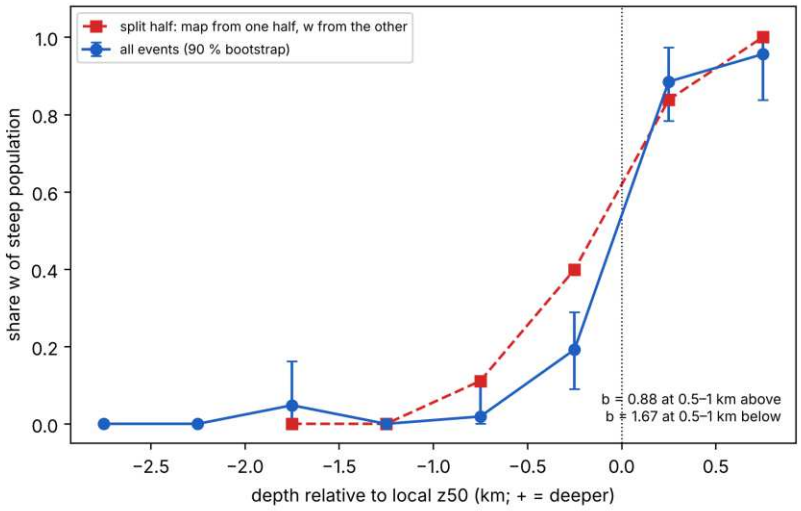


Figure 8. Share w of the steep population against depth relative to the local z50 for all events (blue, 90% bootstrap intervals) and in a split-half test in which z50 was mapped from one half of the events and w measured on the other half (red, post hoc).

4.5 The transition, the seismicity-poor zone and the large earthquakes

Below the busy layer, counts per kilometre fall from 3,961 at 13–14 km to 314 at 15–16 km and rise again at 16–17 km in both the relocated and the JMA catalogue. This seismicity-poor zone at about 14.5–16.5 km corresponds to the aseismic zone in which the geodetic sources of slip and opening lie (Nishimura et al. 2023; Takano et al. 2024); its absolute depth differs by 1–2 km between location procedures (Nakajima 2022). In sections across strike the busy layer (median 12.3 km) and the deep cluster where the swarm began (median 16.75 km) are offset by 5.7 km to the SE, so that the line joining them dips about 38° SE, close to the 43–45° dips of the Suzu fault and the 2023 rupture (Figs. 9–10). Activity crossed the zone in the first months of 2021 (20–32% of events at 14–16 km) and the zone then remained quiet (1–6%). z50 lies 1.4–3.2 km above the top of the zone, which is partly built in by the zone definition. Seen along strike, the zone is a shallow bowl, deepest (≈ 16.2 km) beneath the centre of the busy layer and with a higher SE rim; this shape is robust to the thresholds but partly set by the definition (post hoc, descriptive).

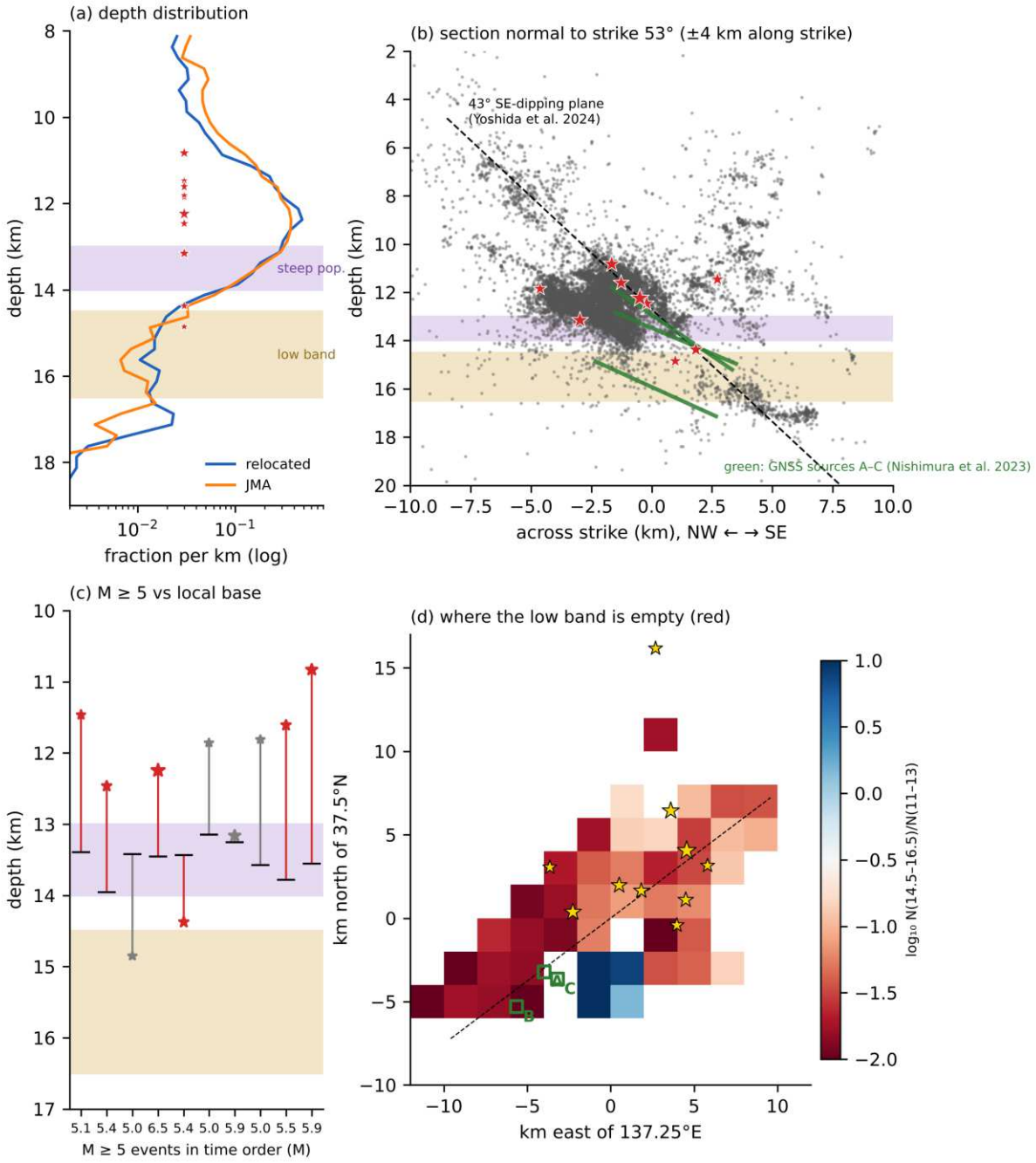


Figure 9. (a) Depth distribution in the relocated and JMA catalogues (December 2020 – 1 January 2024 16:06); stars: M ≥ 5. (b) Section normal to strike 53° with the 43° plane through the 2023 Mj 6.5 and the projected GNSS sources. (c) Depth of each M ≥ 5 event and the local base of seismicity before it (red: first event of a sequence or Mw 7.5 pre-event). (d) Ratio of events at 14.5–16.5 km to 11–13 km in 2-km cells.

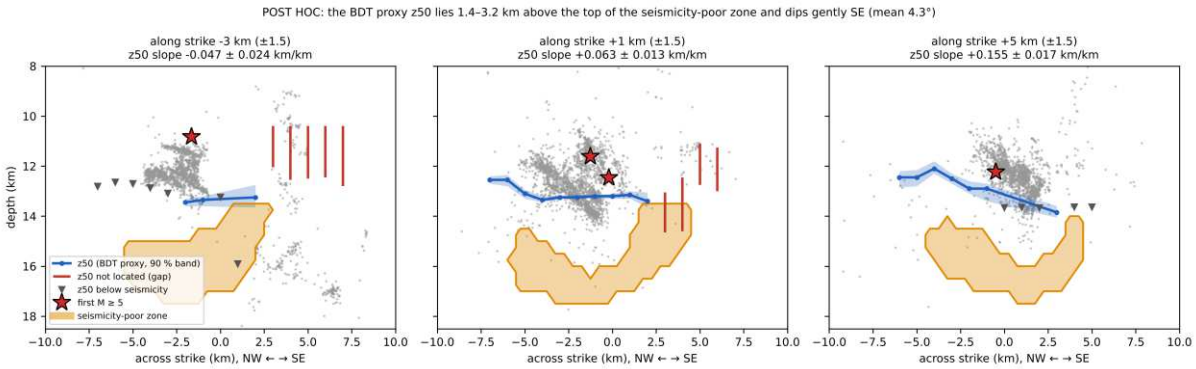


Figure 10. Sections across strike at −3, +1 and +5 km along strike (±1.5 km), seen from the SW (NW left): hypocentres (grey), z50 with its 90% band (blue), nodes where z50 is not located (red bars: gap; triangles: below seismicity), the seismicity-poor zone (orange) and first M ≥ 5 events (stars); titles give the z50 slope of each strip.

All first M ≥ 5 events of each sequence (2021 M 5.1, 2022 M 5.4, 2023 Mj 6.5) and the M 5.5 and M 5.9 pre-events of the 2024 Mw 7.5 nucleated at 10.8–12.5 km, 1.2–2.7 km above the local base of seismicity and 0.5–2.6 km above z50. This is consistent with nucleation in the brittle layer but not distinctive: 86% of all events lie above z50, so five random events would all lie above it with probability ≈ 0.48 (post hoc). The swarm moved 5–6 km up-dip to the NW and 4–5 km upward between late 2020 and 2023; the fault dip, fluid buoyancy and the rise of the transition all point the same way, so the cause of this direction cannot be isolated. Activity did not expand from the onset point as a single front: during the first year the onset cluster stayed within 3–4 km of it, and from mid-February 2021 a group about 8 km away dominated. In a pre-specified comparison of the growth of the 95% distance quantile, diffusive ($r \propto \sqrt{t}$; Shapiro et al. 1997) and constant-velocity growth could not be distinguished by blocked cross-validation of quantile regression (Koenker and Bassett 1978), so we take diffusive migration within clusters from Amezawa et al. (2023) rather than from our fit.

4.6 Is there a b-value precursor?

Table 7. Utsu test of the last 90-day block before the 2024 Mw 7.5 (and, last row, the 2023 Mj 6.5) against the preceding block.

Setting	M_c	Depths	b last block (N)	b previous (N)	ΔAIC	Ordinary blocks ΔAIC > 2
S1 published approach	1.4	all	1.21 (444)	1.05 (471)	+2.61	5/9 (56%)
S2 above M_th	1.8	all	1.01 (133)	0.90 (163)	−1.05	—
S3 step-corrected	1.2	all	0.94 (475)	0.87 (530)	−0.50	—
S4 one layer	1.8	10–13 km	1.07 (90)	0.91 (90)	−0.76	0/7 (0%)
Before Mj 6.5, S1	1.4	all	1.17 (625)	1.25 (888)	−0.50	5/7 (71%)

With the published approach (S1) the last block before the Mw 7.5 has a higher b than the preceding block (1.21 against 1.05; ΔAIC = 2.61), as reported by Li et al. (2024). The same threshold, however, is passed by 56% of ordinary blocks of the same series and by 71% before the Mj 6.5, whose own last block is not significant. Above the processing threshold (S2), with

step-corrected counts (S3) and within one depth layer (S4, no ordinary block significant) the rise is not significant (Table 7, Fig. 11), and in the JMA catalogue the last block lies within the range of earlier blocks for S1 and S4. The pre-specified decision is that a precursor is not supported. The S1 b-values follow the share of deep events in each block (r = 0.84), so at low completeness the b of a block measures mainly how many steep-population events it contains.

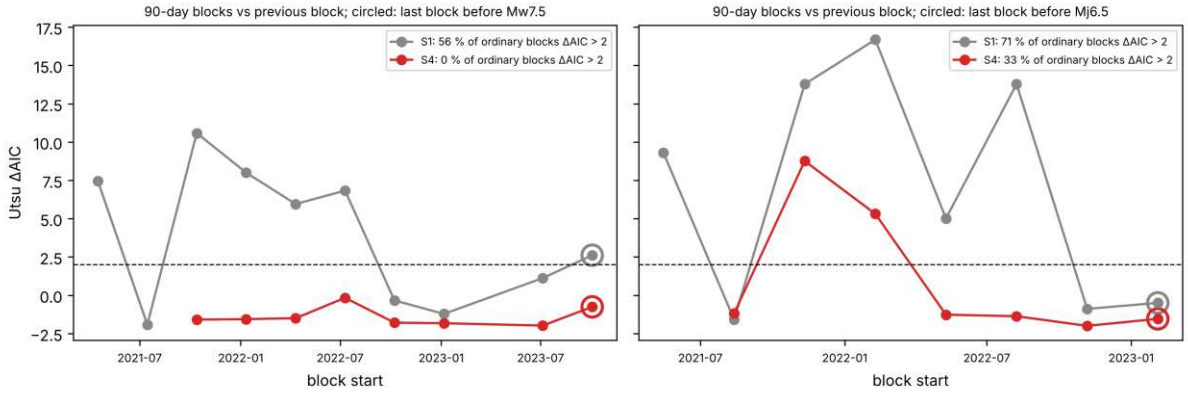


Figure 11. Utsu ΔAIC of each 90-day block against the preceding block before the 2024 Mw 7.5 (left) and the 2023 Mj 6.5 (right) for setting S1 (grey; M_c = 1.4, all depths) and S4 (red; M_c = 1.8, 10–13 km). Circles: last block before the mainshock; dashed line: ΔAIC = 2.

4.7 Seismic velocities, fault dips and helium

In both the Vs model of Takagi, Yoshida and Okada (2025) and the Vp–Vs model of Nakajima (2022) all layers lie in lower velocity than depth-matched random points of the swarm area (Vs −2.5 to −3.7%; Vp −1.5 to −3%; Table 8, Fig. 13). Neither model resolves the layers: Vp/Vs at the layers and in the seismicity-poor zone differs from random points by less than 0.02 (the pre-registered prediction of high Vp/Vs below the busy layer is not met), the Nakajima model has nodes every 5 km in depth, and z50 correlates with neither Vs ($\rho = 0.07$, $p = 0.35$) nor Vp/Vs ($\rho = 0.03$, $p = 0.95$) (Supplementary Figs. S1–S2). The seismogenic faults of the region dip 43–60°, steeper than the frictional optimum (≈ 30°); if differential stress is limited to that which slips an optimal plane at hydrostatic pore pressure, the 43–45° faults need a pore-fluid factor $\lambda_v \approx 0.53$–0.70 and 55–60° faults near-lithostatic pressure (Sibson 1985, 2009; Supplementary Table S1). Faults this steep are poorly oriented for reverse slip and are expected to be reactivated normal faults of the Miocene Japan Sea rift (Sibson 2009; Kato 2024), whereas the geodetic slip planes at the base of the swarm dip only 23–35° and need almost no overpressure (Fig. 12). Mantle helium is strongest at the three sites within 6 km of the deep onset cluster (36–58% mantle helium) and absent above the northern cluster (Supplementary Fig. S3).

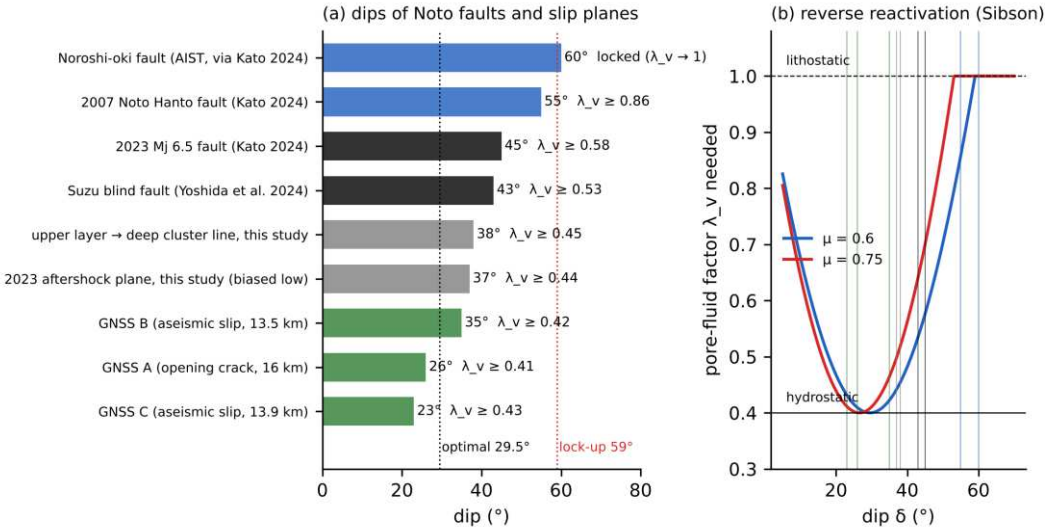


Figure 12. (a) Dips of faults and slip planes in the Noto region with the pore-fluid factor required for reverse slip (μ = 0.6). (b) Required λ_v against dip for μ = 0.6 and 0.75; vertical lines mark the planes of (a).

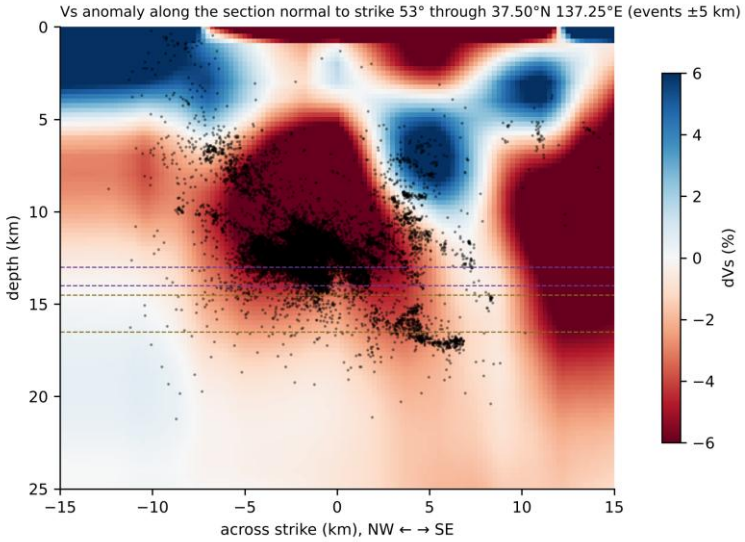


Figure 13. Shear-velocity anomaly along the section normal to strike 53° through 37.50°N 137.25°E (Vs model of Takagi, Yoshida and Okada 2025) with events within ±5 km; dashed lines bound the steep-population layer and the seismicity-poor zone.

Table 8. Mean velocity anomalies at the hypocentres of each layer relative to the regional mean at the same depth. All Vp/Vs differences are below the 0.02 resolution rule.

Layer	N	dVs, Takagi et al. (km/s)	dVp, Nakajima (km/s)	dVs, Nakajima (km/s)	d(Vp/Vs), Nakajima
busy 11–13 km	13,965	−0.126	−0.152	−0.074	−0.007
steep population 13–14 km	3,961	−0.096	−0.197	−0.080	−0.017
seismicity-poor 14.5–16.5 km	674	−0.096	−0.152	−0.055	−0.016
deep cluster 16.5–18 km	404	−0.087	−0.093	−0.035	−0.009

4.8 Is the steep population unique? Comparison across Japan

Before 2016, when all JMA hypocentres were reviewed, R2 found no Noto-type unit among 33 units in Wakayama, northern Yamaguchi, Yamagata–Miyagi and Tohoku, while Noto passed (Δb = +0.62, 95% CI 0.53–0.73). In all seven units with enough events below the base (Wakayama, NW Wakayama, Tohoku inland crust, near Choshi, N Ibaraki, N Miyagi and S Iwate) b fell below the base (Δb = −0.25 to −0.03); the other 26 units had fewer than 150 events below their base, which is sharper than at Noto (Table 9; Supplementary Fig. S8). Thinning Noto to the size of each unit (T2) showed that the signal is detected (power ≥ 0.8) only with about 10,000 or more events above completeness and that thinned Noto is classified as insufficient, never as absent; the seven negative units are therefore informative, whereas northern Yamaguchi (1,100–1,900 events) is not. The opposite curvature of most FMDs ($b_1 < b_2$) was traced mainly to completeness (26 of 48 cases removed by a stricter M_c; 14 more only after 2011), with offshore and slab cases remaining (Supplementary Fig. S9).

In the same era as Noto (T1, 2016–2024, all processing classes) the uniqueness claim failed: Wakayama (three units, Δb = +0.86 to +1.28) and northern Akita (+0.75) were Noto-type (Fig. 14). In Wakayama this signal comes from automatic hypocentres (Δb = +1.01 among them, +0.15 with an interval including zero among reviewed events), a processing-class effect (Section 5.2); at Noto it is strongest among reviewed events (Δb = +1.24, 95% CI 0.97–1.61). Northern Akita also shows it among reviewed events (+0.90, 0.36–2.17, n = 40, post hoc); this area lies near Moriyoshi-zan volcano, with deep low-frequency events and a proposed mid-crustal geofluid reservoir (Kosuga 2014).

Table 9. Pre-registered comparisons of the below-base change of b (Δb = b(h ≥ +1) − b(−3 ≤ h < −1)) between Noto and other JMA areas.

Test (catalogue, period)	Units	Result	Reading
R2, JMA 2000 – Mar 2016 (all reviewed)	33 + Noto control	Noto +0.62 (0.53–0.73); 7 testable units −0.25 to −0.03; 26 insufficient	no other Noto-type unit
T2 power (Noto thinned)	36 target sizes	power ≥ 0.8 from ≈ 10,000 events; never classified absent	negatives informative; N Yamaguchi not
T1, JMA 2016–2024 (all classes)	22 + Noto	Wakayama ×3 (+0.86 to +1.28), N Akita (+0.75) Noto-type	uniqueness falsified
Reviewed events only, 2016–2024 (post hoc)	5	Noto +1.24; N Akita +0.90; Wakayama +0.15 (n.s.); N Ibaraki +0.02	Wakayama signal only in automatic events

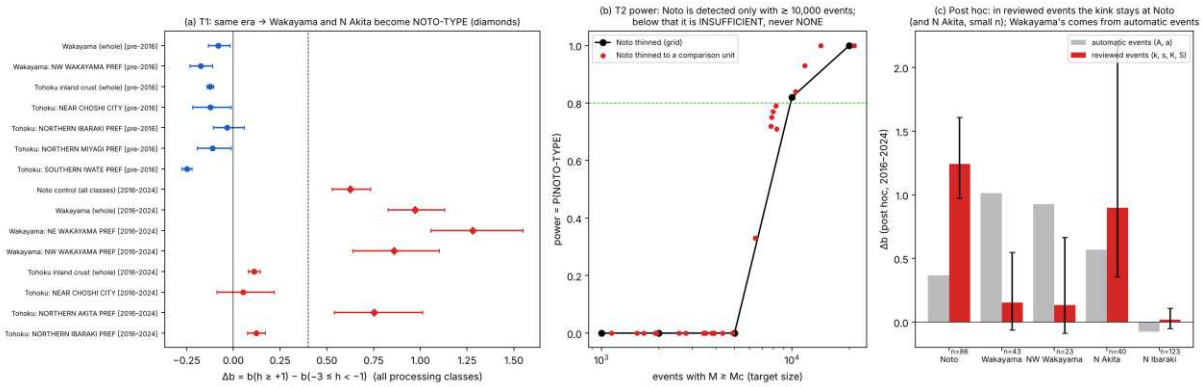


Figure 14. (a) Δb with 95% intervals before 2016 (blue) and in 2016–2024 (red; diamonds: Noto-type). (b) Power: share of random thinnings of Noto classified as Noto-type against the number of events. (c) Δb among automatic (grey) and reviewed (red) events, 2016–2024 (post hoc).

4.9 A volcanic-type signature

Near the active volcanoes of NE Japan, reviewed events after 2016 show b rising below the base (Δb_volc = +0.73, 0.48–1.03, n = 71 below the base), unlike non-volcanic crust (−0.07); the difference (+0.80, 0.55–1.11) met the pre-registered criteria (Table 10, Fig. 15; Supplementary Fig. S12). LFEs make up 36% of the reviewed volcanic events below the base; without them the rise remains (+0.84, 0.53–1.33, n = 42; difference +0.91, 0.60–1.40; post hoc). Noto has no events flagged as LFEs. Before 2016 the pooled volcanic value was negative (−0.16) because 607 of its 703 below-base events come from Kurikoma, the source area of the 2008 Mj 7.2 earthquake (Δb = −0.20); without Kurikoma it was +0.37 (0.14–0.64; post hoc). In an independent, pre-registered replication in Kyushu and Hokkaido the volcanic units again exceeded the non-volcanic ones (+0.42, 0.24–0.62, against +0.08; difference +0.33, 0.10–0.56), just above the thresholds; before 2016 the direction was the same but weaker (+0.18 against −0.08). In this region, however, 55% of the reviewed volcanic events below the base are LFEs. Without them only 38 events remain at the automatic completeness, fewer than the 40 required; with completeness fixed at M 0.4 (post hoc) the rise is +0.44 (0.18–0.86, n = 50; difference +0.36, 0.04–0.80). We therefore regard the Kyushu and Hokkaido result as inconclusive. Keeping the Kumamoto sequence reduced the volcanic value to +0.11, so large tectonic aftershock sequences mask the signal, as at Kurikoma. No single volcano had enough reviewed events below its base for a separate test. The local base of seismicity is deeper at Noto (median D90 of the nodes 14.2 km) than near the NE Japan volcanoes (9.2 km) and similar to that of non-volcanic crust (13.2 km; post hoc).

Table 10. Below-base change of b near active volcanoes (within 15 km) and in non-volcanic crust (> 30 km from all volcanoes).

Group	Period, events	Δb (95% CI), n below base	Pre-registered result
Noto control	2021 – Mj 6.5, reviewed	+1.61 (1.23–2.11), 62	passes

NE Japan volcanic / non-volcanic	2016–2024, reviewed	+0.73 (0.48–1.03), 71 / −0.07 (−0.10 – −0.04), 527	supported (difference +0.80)
NE Japan volcanic, LFEs removed	2016–2024, reviewed	+0.84 (0.53–1.33), 42	post hoc (difference +0.91)
NE Japan volcanic	2000–2016, all	−0.16 (Kurikoma −0.20, 607 of 703); without Kurikoma +0.37 (post hoc)	not supported
Kyushu + Hokkaido volcanic / non-volcanic	2016–2024, reviewed, Kumamoto removed	+0.42 (0.24–0.62), 117 / +0.08 (−0.03 – 0.26), 92	thresholds met (difference +0.33)
Kyushu + Hokkaido volcanic, LFEs removed	2016–2024, reviewed	38 events (< 40); at M_c 0.4: +0.44 (0.18–0.86), 50	post hoc; inconclusive
Kyushu + Hokkaido volcanic / non-volcanic	2000–2016, all	+0.18 (0.09–0.27) / −0.08	same direction, below thresholds

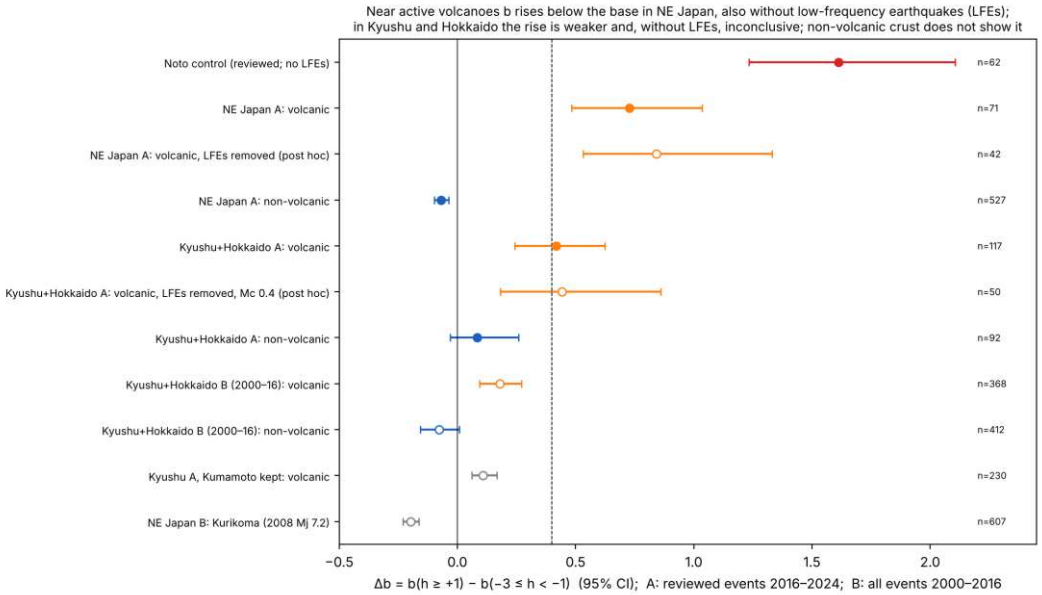


Figure 15. Δb with 95% intervals for Noto, volcanic and non-volcanic groups in NE Japan and in Kyushu and Hokkaido; filled symbols are the pre-registered primary results, open symbols secondary or post hoc results, including groups without low-frequency earthquakes (LFEs); grey: groups dominated by large tectonic aftershock sequences.

4.10 Relation to the Suzu blind fault and to temporal clustering

In the relocated catalogue the steep population (events with h ≥ +1 km before the Mw 7.5) forms a nearly flat layer at 14–18 km beneath the whole swarm. Only 17% of its events lie within 2 km of the SBF plane, against 65–72% for a parallel plane 4 km deeper; 93% lie in the footwall, a median 3.7 km below the plane (pre-registered test P1 not supported for any of four plane geometries; Supplementary Fig. S10). A higher b near the lower edge of the SBF (+0.21) did not survive a ±5° change of dip, and the earlier activation of the steep population (≈ 65 days) was not robust. The steep population is not closer to the initiation of the Mw 7.5 than other deep events (median 8.0 against 7.8 km). After controlling for event density with time-shuffled catalogues, it is as clustered in time as the busy layer (clustering index 0.21 against 0.22; local variation 1.21 against 1.17); raw background fractions (0.70 against 0.64) would have suggested otherwise (Supplementary Fig. S11). The steep population therefore differs from the busy layer in its magnitudes, not in its location on the main fault or in its temporal organisation.

4.11 Independent heat-flow constraint

In NE Japan, sites with a deeper base of seismicity have lower surface heat flow (Spearman ρ = −0.65, one-sided p = 0.001, n = 20), so D90 tracks crustal temperature there (Fig. 16). Only four onshore measurements, all from one 1971 survey, lie within 50 km of the swarm, fewer than the five required, so the direct comparison is insufficient. Their median (97 mW/m²) is lower than within 15 km of the NE Japan volcanoes (161 mW/m², n = 53) and lies within the range of non-volcanic NE Japan (median 82, interquartile range 60–117 mW/m², n = 102); within 100 km of the swarm (post hoc, n = 9) the median is 101 mW/m², lower than near the volcanoes (p = 0.014).

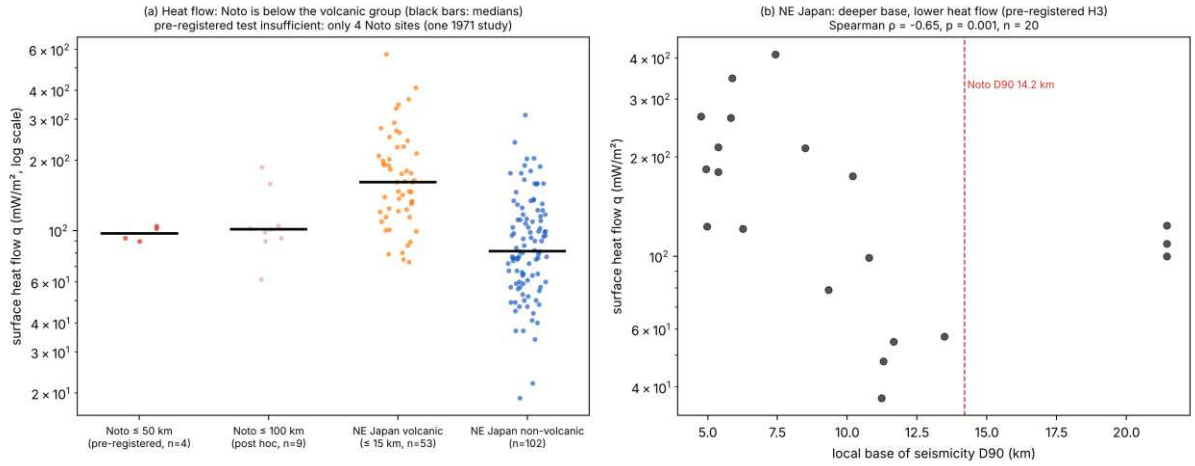


Figure 16. (a) Onshore surface heat flow (Global Heat Flow Database, Release 2024) near Noto (within 50 km, pre-registered; within 100 km, post hoc), within 15 km of the NE Japan volcanoes and in non-volcanic NE Japan; bars are medians. (b) Heat flow against the local base of seismicity D90 at NE Japan sites within 5 km of a D90 node.

5. Discussion

5.1 A layered fault zone

The tests support a layered picture (Fig. 17). Above the transition (10–13 km) one brittle population with b ≈ 0.85–0.95 above M_th occupies the swarm faults; the processing step steepens its FMD below M 1.7 equally in every slice, so the break there is a catalogue feature. Across the transition a population of small events with b ≈ 1.7 — the slope of the deep southern cluster — mixes with the brittle one, and its share rises from a few per cent to about 0.9 within 1 km; because it dominates small magnitudes and the brittle population large ones, the FMD bends with $b_1 > b_2$. Below about 14 km only the steep population remains, with small maximum magnitudes. Seismic slip on small brittle patches in rock that deforms partly aseismically, with high pore pressure (Hirose et al. 2024), would produce such a population; larger events nucleate on continuous faults of the brittle layer (Shelly et al. 2016). Kumazawa and Ogata (2024) also found b increasing with depth within the swarm, and lower stress drops in the medial parts of the northern-cluster faults

(Fukuoka et al. 2024) show fluid-related heterogeneity at the same depths. Rupture-width saturation (Pacheco et al. 1992) acts at much larger magnitudes and has the opposite curvature.

Below the transition the dipping fault zone continues to the deep onset cluster, but the segment between them produced few earthquakes after early 2021, at the depths where geodesy requires aseismic reverse slip and opening. The simplest reading is that this segment slipped largely aseismically — because it lies below the transition, because fluid pressure was high, or both — and loaded the base of the brittle faults, where the large events nucleated, in line with fault-valve behaviour (Sibson 1990, 1992), with swarms and aftershock sequences driven by fluids elsewhere (Miller et al. 2004; Ross et al. 2020) and with the aseismic-slip interpretation of Nishimura et al. (2023). The zone could also partly reflect a velocity-model boundary in the locations or a gap between two structures. The steep inherited faults, reactivated in reverse in an inverted rift setting, require supra-hydrostatic pore pressure, which links fault inversion to the deep fluids indicated by mantle helium. Whether these fluids passed through or were released by an old magmatic body (Okada et al. 2024; Takagi et al. 2025) cannot be decided from hypocentres.

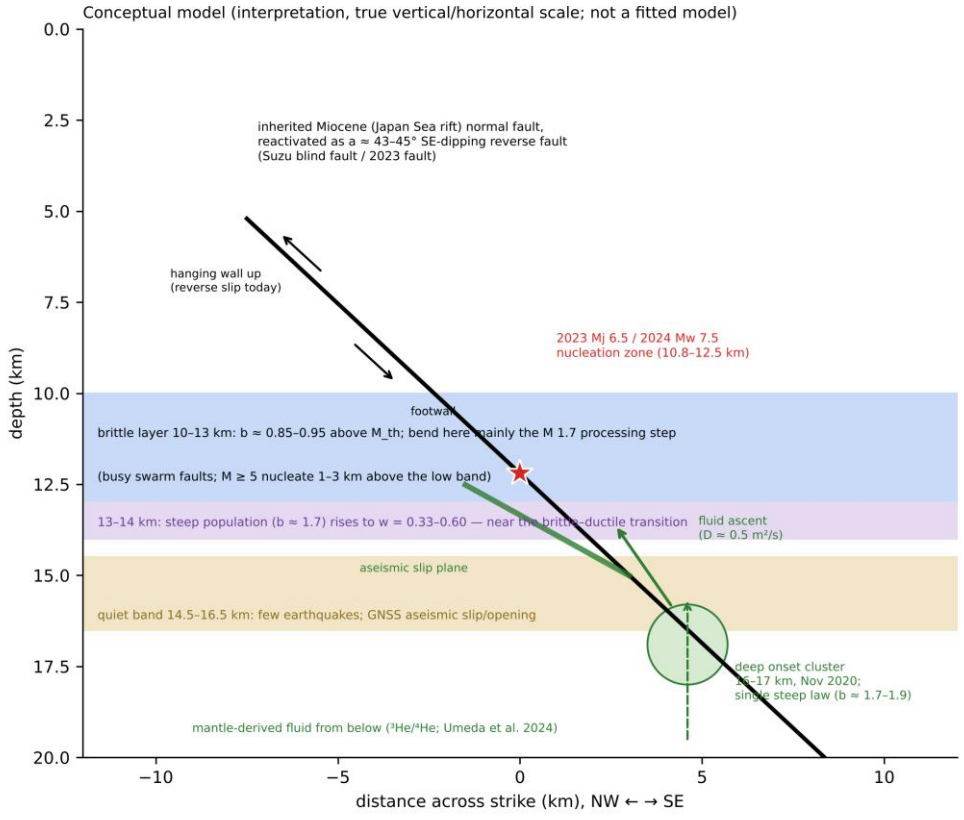


Figure 17. Conceptual cross-section (interpretation, true scale): inherited SE-dipping fault reactivated in reverse; brittle layer with the processing-dominated break; steep small-event population near the brittle–ductile transition (z50); seismicity-poor zone with aseismic slip; deep onset cluster and fluid ascent; nucleation of the large earthquakes in the brittle layer.

The fluids may be of mantle origin. Helium with up to 58% mantle component is found directly above the deep onset cluster (Umeda et al. 2024; Kagoshima et al. 2025), and both velocity models place the swarm in low Vp and Vs. Mantle volatiles can, however, reach the crust without a magma body, and hypocentres cannot distinguish the two. Okada et al. (2024) related high Vp/Vs at about 18 km to a Tertiary magma reservoir, and Takagi et al. (2025) proposed that rupture of solidified ancient magma that had impeded the swarm migration led to the 2024 earthquake; our observations are compatible with fluids rising beneath the southern cluster but cannot decide whether they passed through or were released by such a body. A magmatic origin would require independent evidence, such as an intrusive body imaged at kilometre resolution.

5.2 Catalogue processing classes and depth differences

Automatic hypocentres serve the rapid information service of JMA and are documented as such; the effects below are properties of combining processing classes that users must take into account, not errors of the catalogue. Four observations tie the break at 10–13 km to the JMA processing threshold: the steep branch lies below M_th, where three-quarters of events are automatic; the count ratio across M_th is far below its GR expectation in every band, year and period; the same drop appeared in 2016 in distant regions; and an unrestricted search places the break at 1.7. A uniform shift of automatic magnitudes does not reproduce the shape, whereas an excess of events below 1.7 does, so the effect is more likely in event counts than in magnitudes; re-processing of events whose provisional magnitude reaches M_th is one possibility (Tamaribuchi 2018). The step does not explain why the break depends on depth: it has the same size in slices that bend and in slices that do not, and the processing class and station coverage do not change down to 14 km.

Depth–b profiles from JMA depths differ from those from relocated depths for a related reason. Relative to their relocated positions, automatic hypocentres of M 1.5–1.6 lie 0.16 km shallower and reviewed hypocentres of the same magnitude 0.22 km deeper. Because small events are mostly automatic, JMA depths move small events upward relative to large ones, which raises b at 9–12 km and lowers it at 13–14 km; with relocated depths the same events give b increasing with depth. The high b below 14 km found by Hirose et al. (2024) is not affected.

5.3 Mapping the transition from magnitudes

The transition can be mapped from magnitudes alone, with a node scatter of about ±0.5 km, once the processing step is corrected; its SE deepening is reproduced in an independently located catalogue. We do not claim that z50 is the brittle–ductile transition itself: it is the depth at which a population of small, steep-FMD events becomes dominant, and a temperature, fluid-pressure or rock-type boundary could produce the same change. A transition near 13 km agrees with the

regional cutoff depth (Omuralieva et al. 2012). z50 is not a re-labelled cutoff depth: at the same nodes it correlates only weakly with the 90% depth of seismicity D90 ($\rho = 0.27$; D90 a median 0.4 km deeper), D90 deepens to the SE more than twice as fast because it follows the deep cluster, and where that cluster fell quiet D90 moved up by 2.7–3.6 km between the two halves of the mapping period while z50 changed by ≤ 0.2 km (post hoc). In a pre-registered comparison the median stability of the two measures did not differ (0.10 and 0.11 km), and the better between-catalogue reproducibility of z50 ($\rho = 0.67$ against 0.49) is not significant, so z50 is best regarded as a complementary measure. The SE deepening, steepest near the 2023 Mj 6.5, the 38° line from the busy layer to the deep cluster and the 43–45° faults all describe the same SE-dipping fault zone, but the transition dips only 4–9° and should not be equated with the fault dip. The approach could map transition depths in other dense swarms with relocated catalogues.

5.4 Implications for b-value studies

- b-values of the post-2016 JMA catalogue that span M_th mix processing classes: in this swarm the deep b is 1.45 at M_c = 1.2 but 0.92 at M_c = 1.7. Studies should use M ≥ M_th, correct the step, or check the count ratio across M_th.
- Depth–b profiles from JMA depths differ from those from relocated depths because automatic hypocentres are placed about 0.4 km shallower, relative to relocated positions, than reviewed ones; with relocated depths the decrease of b from 10 to 14 km reported by Hirose et al. (2024) becomes an increase (Supplementary Table S2, Fig. S6).
- In a swarm with a depth-dependent FMD, b changes in time can be produced by the depth mix of events. Precursor claims should report the false-alarm rate of ordinary windows and repeat the test above the processing threshold and within one depth layer.
- In intense swarms the Schuster test of tidal triggering can be inflated several-fold by clustering; a time-shift null removed an apparent tidal signal in the break volume (Supplementary Fig. S5).

5.5 Why Noto? A volcanic-type signature in a non-volcanic swarm

Fluids alone do not produce the steep population: the slab-fluid swarm of Wakayama (Kato et al. 2014) and the fluid-driven 2011 Yamagata–Fukushima swarm (Yoshida et al. 2017) show no rise of b below their base in reviewed data. A rise does occur near the active volcanoes of NE Japan, and less clearly in Kyushu and Hokkaido, and depth-dependent b beneath volcanoes is known (Wiemer and McNutt 1997); what is new here is that the rise is measured relative to the local base of seismicity with one rule across Japan, and that Noto, with no active volcano, shows it more strongly ($\Delta b \approx 1.2$–1.6) than any volcanic group (+0.4 to +0.8). This supports, but does not prove,

the proposal that the Noto fluids leak from a hidden magmatic or deep geofluid system (Yoshida, Uno et al. 2023; Okada et al. 2024), together with the mantle helium and low velocities. The base of seismicity at Noto lies about 5 km deeper than near the NE Japan volcanoes and at a depth similar to non-volcanic crust (Section 4.9). Surface heat flow supports this reading: in NE Japan a deeper base goes with lower heat flow, and the few measurements near Noto are lower than near the volcanoes and within the range of non-volcanic crust (Section 4.11). The Noto crust therefore has a lower geothermal gradient than volcanic areas, so high temperature alone is unlikely to produce the steep population at Noto, and high pore-fluid pressure from a deep, possibly mantle-derived, source is the more consistent explanation; this is a hypothesis. Because Noto shows the strongest rise without volcanic heat, the rise near volcanoes may also be controlled more by fluids than by temperature. Noto also has no LFEs, so its signal does not come from the event type that dominates the volcanic groups of Kyushu and Hokkaido. It does not imply future volcanism, and it does not establish a causal link with the 2024 Mw 7.5: the steep population lies below, not on, the rupture-initiating fault, and the large tectonic sequences at Kurikoma and Kumamoto show the opposite behaviour. The 2025 lower-crustal swarm beneath the Abu volcano group in northern Yamaguchi, 7–17 km below the 2000–2024 base (Amezawa et al. 2026), offers a blind test of this interpretation once its catalogue is released.

5.6 Uncertainties and limitations

We use published catalogues as provided and neither relocate events nor re-estimate magnitudes, so their uncertainties enter every result. Hypocentre depths: relative errors (about 0.13 km) were simulated with Gaussian noise of up to 1 km and shifts of ±1 km, and the main results were repeated in two independently located catalogues; absolute depths differ by 1–2 km between location procedures, so comparisons with velocity models are the least certain. Magnitudes: all are JMA magnitudes, and small-event magnitudes may scale differently from moment magnitude (Deichmann 2006; Uchide and Imanishi 2018), so absolute b-values are catalogue-specific and only differences within one catalogue are interpreted. Processing classes: the step factor was measured outside Noto with a 95% interval of about ±6%, and results were repeated with its upper bound and with reviewed events alone. Completeness: it changes in time and after large events, so periods after the mainshocks were treated separately. Classification: processing classes and LFE flags are taken from JMA, and misclassification would change the volcanic comparison. Sampling: bootstrap intervals assume independent events and are probably too narrow for clustered sequences. Heat flow: only four measurements, from one 1971 survey, lie near the swarm, and surface heat flow does not give the temperature at 10–15 km directly; new borehole

measurements at Noto would test the thermal argument. Multiple testing: many tests were run; pre-registered tests are separated from post hoc ones, which should be read as exploratory.

The break was found by exploring the data; the processing audit, the depth-slice tests, the node quality rule, the split-half test and the relation to the seismicity-poor zone were post hoc. All magnitudes are JMA magnitudes; no independent moment magnitudes exist for small events. Single z50 nodes scatter by ±0.5 km, the JMA transition is 0.9 km deeper and the eastern deepening was not replicated. Absolute depths differ by 1–2 km between location procedures, so the layers should be read relative to the clusters. Only five large-event sequences and 6–9 ordinary 90-day blocks per series are available. The processing-class test is limited to M 1.5–1.6 because JMA flags were used only for $M \geq 1.5$, and the Wakayama replication uses JMA, not relocated, depths. The catalogue ends in March 2024. The volcanic interpretation rests on pooled groups (71 and 117 reviewed events below the base), only just met the thresholds in Kyushu and Hokkaido and became inconclusive there without LFEs, uses reviewed events whose absolute b is biased by magnitude-dependent selection (only differences are interpreted), and arose from a post hoc observation in northern Akita.

6. Conclusions

- The deep FMD kink of the Noto swarm is real. After correcting the JMA M 1.7 processing step, it vanishes at 10–13 km but survives below 13 km, where a steep small-event population ($b \approx 1.7$) rises to 33–60% within 1 km and persisted from 2021 to late 2023; it is present in reviewed events alone.
- An event-level mixture model maps the onset depth of this population, a brittle–ductile transition proxy, at 12.45–13.5 km; it varies laterally, deepens 4.3° to the SE and is reproduced by the JMA catalogue. A seismicity-poor zone below it coincides with the geodetic aseismic zone.
- The steep population lies 3–5 km below the Suzu blind fault, not on it, and is no less clustered in time than the layer above.
- With one pre-registered rule, b falls below the base of seismicity in non-volcanic Japanese crust but rises near the active volcanoes of NE Japan, also without low-frequency earthquakes; in Kyushu and Hokkaido the rise is weaker and inconclusive. Noto, with no low-frequency earthquakes and a deeper base, shows the strongest rise, a volcanic-type signature in a non-volcanic swarm that we tentatively attribute to high fluid pressure from a deep source; surface heat flow there is lower than near volcanoes.

- The b-value rise reported before the 2024 Mw 7.5 is matched by half or more of ordinary blocks and disappears above the processing threshold; no causal or precursory link of the steep population to the Mw 7.5 is established.
- Moment magnitudes of small events, relocated catalogues of volcanic areas and the 2025 northern Yamaguchi swarm are needed to test the interpretation further.

Abbreviations

BDT: brittle–ductile transition; BIC: Bayesian information criterion; FMD: magnitude–frequency distribution; D90: 90% depth of seismicity; GR: Gutenberg–Richter; JMA: Japan Meteorological Agency; LFE: low-frequency earthquake; M_c: completeness magnitude; M_k: break magnitude; M_th: JMA processing threshold magnitude; z50: depth at which the steep population makes up half of the events.

Declarations

Availability of data and materials

The relocated catalogue is available from Zenodo (doi 10.5281/zenodo.12799165; CC BY 4.0) and the JMA unified hypocentre catalogue from the Japan Meteorological Agency. The comparison catalogues are available from github.com/sadeghkarimpouli/Family_based_features (commit 5e67f5a) and GFZ Data Services (doi 10.5880/GFZ.4.1.2023.004), the Vs model from Dryad (doi 10.5061/dryad.zcrjdfnm3), the heat-flow data from the Global Heat Flow Database (GFZ Data Services, doi 10.5880/fidgeo.2024.014; CC BY 4.0), and the Vp–Vs model from the laboratory of J. Nakajima (not redistributed); the JMA area extracts used for the comparisons are derived from the public JMA catalogue. All scripts, protocols with SHA-256 fingerprints, analysed event tables and figures are provided in the reproducibility packages listed in the Supplementary Information and will be deposited in a public repository on acceptance.

Competing interests

The authors declare no competing interests.

Funding

This research received no external funding.

Author contributions

R.P. designed the study, performed the analyses and wrote the manuscript. R.M. contributed to the analysis and its further improvement. P.J.V.R. helped draft the manuscript.

Acknowledgements

We thank K. Yoshida and co-authors for their relocated catalogue, the Japan Meteorological Agency for the unified hypocentre catalogue, F. Hirose and colleagues for TidalStrain.2, S. Karimpouli and co-authors and GFZ Data

Services for the comparison catalogues, J. Nakajima for the P- and S-wave model, R. Takagi, K. Yoshida and T. Okada for the S-wave model, and the Global Heat Flow Data Assessment Group for the heat-flow database.

References

Aki K (1965) Maximum likelihood estimate of b in the formula log N = a − bM and its confidence limits. Bull Earthq Res Inst 43:237–239

Amezawa Y, Hiramatsu Y, Miyakawa A, Imanishi K, Otsubo M (2023) Long-living earthquake swarm and intermittent seismicity in the northeastern tip of the Noto Peninsula, Japan. Geophys Res Lett 50:e2022GL102670

Amezawa Y, Yabe S, Sawaki Y, Imanishi K, Miyazawa M, Nishikawa T, Nishimura T, Nagaoka A, Miyamachi R, Ohmi S (2026) Deep crustal earthquake swarm and complex seismicity migrations in northern Yamaguchi, southwestern Japan. EGU General Assembly 2026, EGU26-15500 (abstract)

Aochi H (2024) Dynamic rupture inversion on the M5.9 pre-event before the 2024 M7.6 Noto-Peninsula, Japan, earthquake. Earth Planets Space 76. https://doi.org/10.1186/s40623-024-02095-4

Deichmann N (2006) Local magnitude, a moment revisited. Bull Seismol Soc Am 96:1267–1277

Fukuoka M, Hiramatsu Y, Yamada T (2024) Linking the spatiotemporal distribution of static stress drops to source faults in a fluid-driven earthquake swarm, northeastern Noto Peninsula, central Japan. Earth Planets Space 76:125. https://doi.org/10.1186/s40623-024-02074-9

Global Heat Flow Data Assessment Group et al. (2024) The Global Heat Flow Database: Release 2024, version 2026.03. GFZ Data Services. https://doi.org/10.5880/fidgeo.2024.014

Gulia L, Wiemer S (2019) Real-time discrimination of earthquake foreshocks and aftershocks. Nature 574:193–199

Gutenberg B, Richter CF (1944) Frequency of earthquakes in California. Bull Seismol Soc Am 34:185–188

Hirose F, Maeda K, Kamigaichi O (2019) Tidal forcing of interplate earthquakes along the Tonga-Kermadec Trench. J Geophys Res Solid Earth 124:10498–10521. https://doi.org/10.1029/2019JB018088

Hirose F, Tamaribuchi K, Kobayashi A, Maeda K (2024) Relation between earthquake swarm activity and tides in the Noto region, Japan. Earth Planets Space 76:37. https://doi.org/10.1186/s40623-024-01985-x

Japan Meteorological Agency. Notes on the JMA unified hypocentre catalogue. https://www.data.jma.go.jp/eqev/data/bulletin/catalog/notes_e.html

Kagoshima T et al (2025) Helium isotope anomaly in groundwater prior to the 2024 Noto Peninsula earthquake. Nat Commun 16. https://doi.org/10.1038/s41467-025-65717-9

Karimpouli S et al (2026) Nature Communications 17:4024 (catalogues: https://github.com/sadeghkarimpouli/Family_based_features)

Kato A (2024) Implications of fault-valve behavior from immediate aftershocks following the 2023 Mj6.5 earthquake beneath the Noto Peninsula, central Japan. Geophys Res Lett 51:e2023GL106444

Kato A, Saiga A, Takeda T (2014) Non-volcanic seismic swarm and fluid transportation driven by subduction of the Philippine Sea slab beneath the Kii Peninsula, Japan. Earth Planets Space 66:86

Koenker R, Bassett G (1978) Regression quantiles. Econometrica 46:33–50. https://doi.org/10.2307/1913643

Kosuga M (2014) Seismic activity near the Moriyoshi-zan volcano in Akita Prefecture, northeastern Japan: implications for geofluid migration and a midcrustal geofluid reservoir. Earth Planets Space 66:77. https://doi.org/10.1186/1880-5981-66-77

Kumazawa T, Ogata Y (2024) Spatial and temporal variations of the 3-year earthquake swarm activities leading up to the M7.6 Noto Peninsula earthquake and interpretations of their activities. Earth Planets Space 76:164. https://doi.org/10.1186/s40623-024-02112-6

Li W, Yoshino C, Hattori K (2024) Study of the b-value change preceding the 2024 Noto Peninsula earthquake M7.6, Japan. Seismological Society of America Annual Meeting 2024, poster presentation

Miller SA, Collettini C, Chiaraluce L, Cocco M, Barchi M, Kaus BJP (2004) Aftershocks driven by a high-pressure CO2 source at depth. Nature 427:724–727

Mohanna S, Meng L, Vuan A, Yu H (2026) Swarm cessation and aftershock drivers following the pressure release of a four-year-long seismic sequence at the Noto Peninsula. Earth Planet Sci Lett 690:120113

Mori J, Abercrombie RE (1997) Depth dependence of earthquake frequency-magnitude distributions in California: implications for rupture initiation. J Geophys Res 102:15081–15090

Nakajima J (2022) Crustal structure beneath earthquake swarm in the Noto peninsula, Japan. Earth Planets Space 74:160. https://doi.org/10.1186/s40623-022-01719-x

Nishimura T, Hiramatsu Y, Ohta Y (2023) Episodic transient deformation revealed by the analysis of multiple GNSS networks in the Noto Peninsula, central Japan. Sci Rep 13:8381

Okada T, Savage MK, Sakai S, Yoshida K, Uchida N, Takagi R, Kimura S, Hirahara S, Tagami A, Fujimura R, Matsuzawa T, Kurashimo E, Hiramatsu Y (2024) Shear wave splitting and seismic velocity structure in the focal area of the earthquake swarm and their relation with earthquake swarm activity in the Noto Peninsula, central Japan. Earth Planets Space 76. https://doi.org/10.1186/s40623-024-01974-0

Omuralieva AM, Hasegawa A, Matsuzawa T, Nakajima J, Okada T (2012) Lateral variation of the cutoff depth of shallow earthquakes beneath the Japan Islands and its implications for seismogenesis. Tectonophysics 518–521:93–105

Pacheco JF, Scholz CH, Sykes LR (1992) Changes in frequency–size relationship from small to large earthquakes. Nature 355:71–73

Ross ZE, Cochran ES, Trugman DT, Smith JD (2020) 3D fault architecture controls the dynamism of earthquake swarms. Science 368:1357–1361

Scholz CH (1968) The frequency-magnitude relation of microfracturing in rock and its relation to earthquakes. Bull Seismol Soc Am 58:399–415

Schorlemmer D, Wiemer S, Wyss M (2005) Variations in earthquake-size distribution across different stress regimes. Nature 437:539–542

Schuster A (1897) On lunar and solar periodicities of earthquakes. Proc R Soc Lond 61:455–465

Shapiro SA, Huenges E, Borm G (1997) Estimating the crust permeability from fluid-injection-induced seismic emission at the KTB site. Geophys J Int 131:F15–F18

Shelly DR, Ellsworth WL, Hill DP (2016) Fluid-faulting evolution in high definition: connecting fault structure and frequency-magnitude variations during the 2014 Long Valley Caldera, California, earthquake swarm. J Geophys Res Solid Earth 121:1776–1795. https://doi.org/10.1002/2015JB012719

Shi Y, Bolt BA (1982) The standard error of the magnitude-frequency b value. Bull Seismol Soc Am 72:1677–1687

Shinomoto S, Shima K, Tanji J (2003) Differences in spiking patterns among cortical neurons. Neural Comput 15:2823–2842

Sibson RH (1985) A note on fault reactivation. J Struct Geol 7:751–754

Sibson RH (1990) Conditions for fault-valve behaviour. In: Knipe RJ, Rutter EH (eds) Deformation mechanisms, rheology and tectonics. Geol Soc Lond Spec Publ 54:15–28

Sibson RH (1992) Implications of fault-valve behaviour for rupture nucleation and recurrence. Tectonophysics 211:283–293

Sibson RH (2009) Rupturing in overpressured crust during compressional inversion — the case from NE Honshu, Japan. Tectonophysics 473:404–416

Spada M, Tormann T, Wiemer S, Enescu B (2013) Generic dependence of the frequency-size distribution of earthquakes on depth and its relation to the strength profile of the crust. Geophys Res Lett 40:709–714

Takagi R et al (2025) Rupture of solidified ancient magma that impeded preceding swarm migrations led to the 2024 Noto earthquake. Sci Adv 11:eadv5938. https://doi.org/10.1126/sciadv.adv5938

Takagi R, Yoshida K, Okada T (2025) Ambient noise cross-correlation functions and three-dimensional S-wave velocity structure in the Noto Peninsula, Japan. Dryad. https://doi.org/10.5061/dryad.zcrjdfnm3

Takano S, Hiramatsu Y, Yukutake Y (2024) The role of fluids in earthquake swarms in northeastern Noto Peninsula, central Japan: insights from source mechanisms. Earth Planets Space 76:151. https://doi.org/10.1186/s40623-024-02099-0

Tamaribuchi K (2018) Evaluation of automatic hypocenter determination in the JMA unified catalog. Earth Planets Space 70:141. https://doi.org/10.1186/s40623-018-0915-4

Uchide T, Imanishi K (2018) Underestimation of microearthquake size by the magnitude scale of the Japan Meteorological Agency: influence on earthquake statistics. J Geophys Res Solid Earth 123

Umeda K, Yamazaki Y, Sumino H (2024) Geochemical signature of deep fluids triggering earthquake swarm in the Noto Peninsula, central Japan. Geophys Res Lett 51. https://doi.org/10.1029/2024GL108581

Utsu T (1965) A method for determining the value of b in a formula log n = a − bM showing the magnitude-frequency relation for earthquakes. Geophys Bull Hokkaido Univ 13:99–103

Utsu T (1992) On seismicity. In: Report of the Joint Research Institute for Statistical Mathematics, Institute of Statistical Mathematics, Tokyo 34:139–157

Wiemer S, McNutt SR (1997) Variations in the frequency-magnitude distribution with depth in two volcanic areas: Mount St. Helens, Washington, and Mt. Spurr, Alaska. Geophys Res Lett 24:189–192

Wiemer S, Wyss M (2000) Minimum magnitude of completeness in earthquake catalogs. Bull Seismol Soc Am 90:859–869

Xu L, Ji C, Meng L, Ampuero J-P, Yunjun Z, Mohanna S, Aoki Y (2024) Dual-initiation ruptures in the 2024 Noto earthquake encircling a fault asperity at a swarm edge. Science 385:871–876. https://doi.org/10.1126/science.adp0493

Yoshida K, Saito T, Urata Y, Asano Y, Hasegawa A (2017) Temporal changes in stress drop, frictional strength, and earthquake size distribution in the 2011 Yamagata-Fukushima, NE Japan, earthquake swarm, caused by fluid migration. J Geophys Res Solid Earth 122:10379–10397

Yoshida K, Takagi R, Fukushima Y, Ando R, Ohta Y, Hiramatsu Y (2024) Role of a hidden fault in the early process of the 2024 Mw7.5 Noto Peninsula earthquake. Geophys Res Lett 51:e2024GL110993. Dataset: https://doi.org/10.5281/zenodo.12799165

Yoshida K, Uno M, Matsuzawa T, Yukutake Y, Mukuhira Y, Sato H, Yoshida T (2023) Upward earthquake swarm migration in the northeastern Noto Peninsula, Japan, initiated from a deep ring-shaped cluster: possibilities of fluid leakage from a hidden magma system. J Geophys Res Solid Earth 128:e2022JB026047

Zaliapin I, Ben-Zion Y (2013) Earthquake clusters in southern California I: identification and stability. J Geophys Res Solid Earth 118:2847–2864